Global and Planetary Change 199 (2021) 103446

Contents lists available at ScienceDirect

Global and Planetary Change

journal homepage: www.elsevier.com/locate/gloplacha

Research article

Multi-method comparison of modern river sediments in the Pannonian Basin System – A key step towards understanding the provenance of sedimentary basin-fill

Róbert Arató [a,*], Gabriella Obbágy [a], István Dunkl [b], Sándor Józsa [c], Keno Lünsdorf [b], János Szepesi [a,d], Kata Molnár [a], Zsolt Benkó [a], Hilmar von Eynatten [b]

[a] Isotope Climatology and Environmental Research Centre, Institute for Nuclear Research, Hungarian Academy of Sciences, Debrecen, Hungary
[b] Department of Sedimentology and Environmental Geology, University of Göttingen, Germany
[c] Department of Petrology and Geochemistry, Eötvös Loránd University, Budapest, Hungary
[d] MTA-ELTE Volcanology Research Group, Budapest, Hungary

ARTICLE INFO

Keywords:
Provenance
Thermochronology
Apatite fission-track analysis
Zircon fission-track analysis
Heavy mineral analysis
Fine-gravel petrography
Pannonian Basin
Alps
Carpathians

ABSTRACT

We compared the sedimentary provenance signature of modern river sediments collected from 14 different rivers entering the Pannonian Basin. The Pannonian Basin is one of the largest sedimentary basins of Europe filled up by multiple potential sediment sources. However, the contribution of individual source areas is unknown and complex basin-fill mixtures can only be disentangled by the knowledge of more simple mixtures such as modern river sediments. Our goal was to obtain a multi-parameter dataset about modern river sediments and potential source areas as well as to identify effects that can modify primary signatures, such as recycling. We simultaneously applied zircon and apatite fission-track detrital thermochronology (ZFT and AFT, respectively), heavy mineral analysis (HMA) via automated Raman spectroscopy and fine gravel petrography (FGP). ZFT ages cover a broader age range and show more significant dissimilarities between different rivers, than the AFT ages that mostly record the latest, Neogene cooling event of the source areas. On the other hand, heavy mineral spectra can be roughly subdivided into metamorphic, igneous and recycled signatures. Based on the amount of ultrastable minerals and the areal extent of different sedimentary reservoirs in each catchment, we can also estimate their relative contribution to recycling. Furthermore, simultaneous application of heavy mineral analysis and thermochronology with proper statistical treatment enables to distinguish specific source areas and mixed sedimentary signatures. The results provide a methodological basis for future reconstructions of tectonic and climate-based changes in the source area from mixed basin-fill sediments on a million-year scale.

1. Introduction

Sedimentary basins act as a sink for the material eroded from adjacent mountains and thus their sedimentary fill provides the missing piece of information to understand the evolution of the sediment routing system (e.g. Carter, 2007; Malusà and Balestrieri, 2012).

The Alpine-Carpathian realm is a set of geodynamically interconnected sediment sources and sinks with a continuously changing post-collisional evolution history in space and time from the Oligocene until recent (e.g. Kuhlemann et al., 2002; Schmid et al., 2008; Matenco and Andriessen, 2013). During the late Miocene and Pliocene, the vast majority of the eroded material from the Eastern Alps, the Bohemian Massif and the Carpathians was delivered to the Pannonian Basin (Kuhlemann et al., 2002). This resulted in the accumulation of thick (>6 km) basin-fill (e.g. Horváth et al., 2015), making the Pannonian Basin one of the largest sedimentary basins of the continent. The basin-fill can be interpreted as a complex mixture of several paleorivers' sediments, which originate at least from six major source areas, namely the Eastern Alps, the Bohemian Massif, the Western Carpathians, the Eastern Carpathians, the Southern Carpathians and the Apuseni Mountains (Fig. 1a). Despite prior efforts to unravel the provenance of sediment mixtures within the basin via heavy mineral analysis (HMA; Juhász and Thamó-Bozsó, 2006; Thamó-Bozsó et al., 2006), it remains unclear to what extent each potential source area contributed to them.

* Corresponding author.
E-mail address: arato.robert@atomki.mta.hu (R. Arató).

https://doi.org/10.1016/j.gloplacha.2021.103446
Received 16 March 2020; Received in revised form 2 February 2021; Accepted 4 February 2021
Available online 10 February 2021

Modern river sediments represent the primary components of the Miocene-Quaternary (e.g. Magyar et al., 2013) basin-fill and assessing these mixtures is therefore essential for understanding more complex sediments. Differentiation between potential sources is challenging for multiple reasons. Various stages of sediment recycling in Cretaceous, Paleogene and Miocene siliciclastic sediments (Fig. 1b) can result in reset fission-track ages (e.g. Nakapelyukh et al., 2018) as well as in modifications of heavy mineral contents (e.g. Di Giulio et al., 2003). Further difficulties are introduced by the nature of the study area, which raise the question if the studied sediments are distinguishable at all: (i) the entire Alpine-Carpathian realm shares a similar evolution history with largely similar fission-track (FT) ages and/or bedrock composition (Figs. 1 and 2) and (ii) modern rivers drain multiple terranes and carry a mixed detrital signal.

In order to link primary sediments to bedrock, describe the detrital signature of potential source areas and estimate the relative contribution of different sedimentary units to recycling, in this study we compare modern river sediments with respect to their detrital zircon fission-track (ZFT) and apatite fission-track (AFT) ages as well as their heavy mineral (HM) spectra and fine gravel (FG) content. This study is also an attempt to exploit the high discriminating potential of multi-method provenance analysis combined with multi-parameter statistical treatment. Moreover, with our new detrital ZFT, AFT, heavy mineral and petrographic dataset we make a crucial step towards understanding the complex basin-fill of the Pannonian Basin.

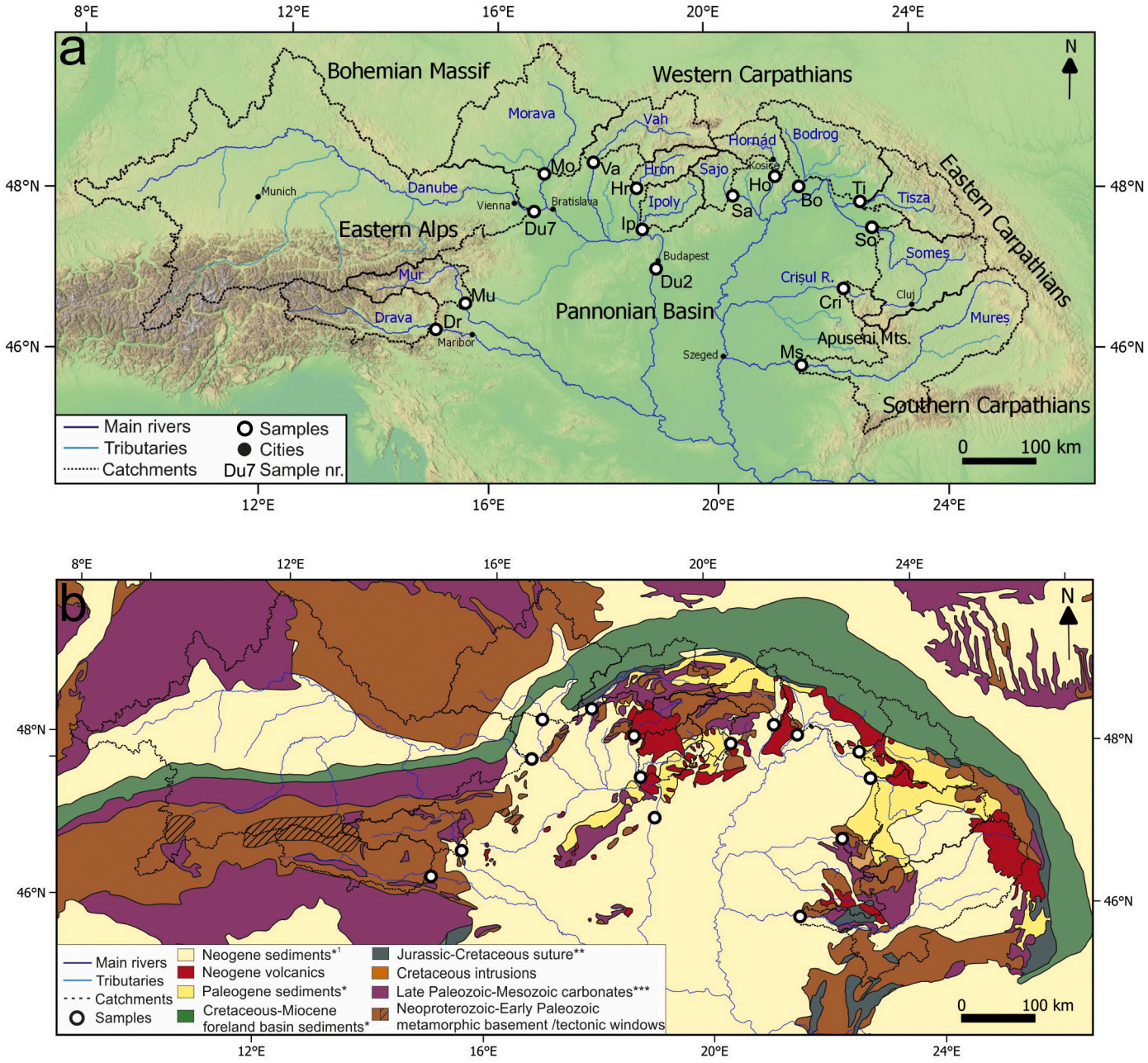

Fig. 1. (a) Topographic map of the study area and the catchments of sampled rivers with the sampling sites. (b) Geological map of the study area (simplified after Asch, 2003). *clastic sediments **carbonates in the Western and Eastern Carpathians and ophiolites (+carbonates) in the Apuseni Mts. and Southern Carpathians ***also subordinately/locally clastic sediments. [1]Neogene and also Quaternary sediments.

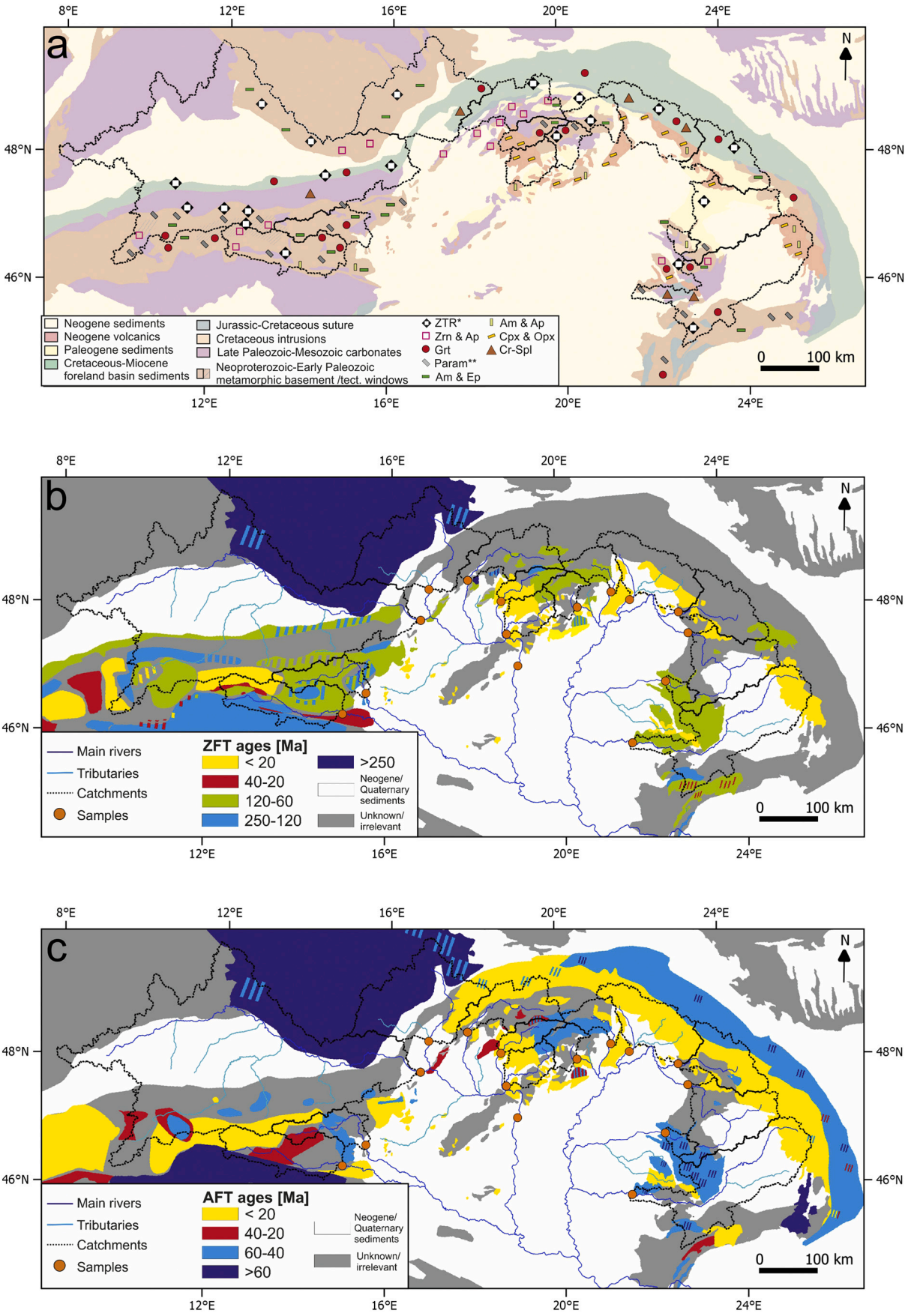

(caption on next page)

Fig. 2. (a) Bedrock heavy mineral content compilation *zircon, tourmaline, rutile, ** sillimanite, kyanite, staurolite, chloritoid; Zrn = zircon, Ap = apatite, Grt = garnet, Ep = epidote, Am = amphibole Cpx = clinopyroxene, Opx = orthopyroxene, Cr-Spl = chromian spinel, (b) Zircon and (c) apatite bedrock fission-track age compilation based on Grundmann and Morteani (1985), Flisch (1986), Hurford (1986), Staufenberg (1987), Hejl and Grundmann (1989), Neubauer et al. (1995), Fügenschuh et al. (1997), Hejl (1997), Dunkl et al. (1998), Elias (1998), Sachsenhofer et al. (1998), Stöckhert et al. (1999), Trautwein et al. (2001), Viola et al. (2001), Dunkl et al. (2009) [Alps]; Hejl et al. (1997, 2003), Glasmacher et al. (2002), Vamvaka et al. (2014), Botor et al. (2017), Sobczyk et al. (2020) [Bohemian Massif]; Burchart (1972), Král (1977), Kováč et al. (1994), Danišík et al. (2004, 2008a, 2008b, 2010, 2011, 2012), Plašienka et al. (2007), Zattin et al. (2011), Andreucci et al. (2013), Králiková et al. (2014a, 2014b, 2016), Anczkiewicz et al. (2015), Śmigielski et al. (2016), Vojtko et al. (2016) [Western Carpathians]; Sanders et al. (1999), Merten et al. (2010), Gröger et al. (2013), Andreucci et al. (2015), Nakapelyukh et al. (2018) [Eastern Carpathians]; Bojar et al. (1998), Schmid et al. (1998), Moser et al. (2005), Fügenschuh and Schmid (2005), Matenco (2017) [Southern Carpathians]; Schuller (2004), Schuller et al. (2009), Merten et al. (2011), Kounov and Schmid (2013), Reiser et al. (2017) [Apuseni Mountains]. Neogene volcanics are automatically categorized as <20 Ma. Striped areas indicate sporadic occurrences or mixed/transitional FT age populations.

2. Geological background

2.1. The Alpine-Carpathian-Pannonian source to sink system

The 800,000 km^2 catchment area of the modern Danube river covers a significant part of the European continent, spanning from the Eastern Alpine foreland to the Black Sea. Its tributaries drain diverse geological units from several major mountain belts of the region, including the Eastern Alps, the Bohemian Massif, the Carpathians and the Apuseni Mountains (Fig. 1). The complex structure of these orogens reflects a superposition of multiple mountain-building events that can be traced back from recent times to the Paleozoic (e.g. Frisch, 1979; Stampfli et al., 1991; Csontos and Vörös, 2004). Large parts of the crystalline basement in the Alps and Carpathians as well as the Bohemian Massif formed during the Late Ordovician – Late Carboniferous Variscan orogeny (e.g. Franke, 2000). Subsequent Cretaceous-Paleogene collision and nappe-stacking of the African and Eurasian continents is related to the Jurassic subduction of the Neotethys ocean (e.g. Frisch, 1979), commonly referred to as the Eoalpine event. This event partly overlaps with the Cretaceous-Eocene closure of the Alpine Tethys Ocean (e.g. Bertotti et al., 1999), subsequent collision and exhumation ("Neoalpine event").

The Oligocene to recent post-collisional evolution history of the Eastern Alps and Carpathians was accompanied by the gradual eastward migration of the dominant sinks of eroded sediments. The foreland basin of the Alps served as the major sink of Eastern Alpine detritus from the Oligocene (ca. 30 Ma) until the late Miocene (ca. 11–10 Ma; Kuhlemann and Kempf, 2002) when the main depocenter was shifted to the Pannonian Basin. Accordingly, the Pannonian Basin stores most of the material that was eroded from the Eastern Alps, the Bohemian Massif and Carpathians between the late Miocene (ca. 11–10 Ma) and late Pliocene (Kuhlemann et al., 2002). Sediments were delivered to the basin by several rivers from different directions, most probably including the precursor of the Danube (Magyar et al., 2013). It is clear from changing shelf-margin progradation directions (Magyar et al., 2013) that the source of sediments changed multiple times between 10 and 4 Ma. This is also supported by differences in the detrital (apatite and zircon) fission-track age distributions (Tari et al., 1999) and HM association of the basin-fill (Thamó-Bozsó et al., 2006).

Several modern river sediments in the study area were also investigated in prior studies with respect to their HM assemblage (e.g. Szabó, 1955; Molnár, 1964; Gedeon-Rajetzky, 1973; Thamó-Bozsó and Kovács, 2007). Thamó-Bozsó and Kovács (2007) could distinguish the HM signature of Danube and Tisza (and most of their tributaries) via principal component analysis, identify characteristic features of the Carpathians and Apuseni Mountains in detrital material and also explain the origin of certain Quaternary sediments in boreholes.

2.2. Geology and characteristic lithologies of the potential source areas

The information described in this section is summarized in Fig. 1b and Table S1.

2.2.1. Bohemian Massif

The Bohemian Massif represents the relatively stable central European crust consolidated during the Variscan orogeny (e.g. Franke and Żelaźniewicz, 2002), in contrast to the much younger Alpine-Carpathian mountain chain (Figs. 1, 2). It is dominated by variably metamorphosed Neoproterozoic to Lower Paleozoic volcano-sedimentary successions and igneous complexes, Variscan (ca. 350–300 Ma; e.g. Klein et al., 2008; Janoušek et al., 2010) felsic to ultrapotassic igneous rocks as well as by Upper Cretaceous sediments.

2.2.2. Eastern Alps

The Eastern Alps are dominated by a multiply deformed basement and its weakly metamorphosed cover nappes of African origin (e.g. Froitzheim and Manatschal, 1996; Fig. 1b). Their continuation also comprises the basement of the northern Pannonian Basin (Balla, 1984). Basement units consist of predominantly (Neoproterozoic–)Paleozoic amphibolite and greenschist facies metamorphic rocks with eclogitic occurrences along the Mur River (e.g. Miller et al., 2005). Their Mesozoic cover sequences in the north are dominated by carbonates.

Tectonic windows (Fig. 1b) expose Europe-derived continental sequences and their cover units related to the Cretaceous-Eocene Alpine Tethys closure (e.g. Frisch, 1979). Their lithology spans a range from greenschist and amphibolite facies rocks (Fig. 2a) to widespread blueschists and subordinate eclogite facies rocks (e.g. Bousquet et al., 2008).

The northern foreland of the Alps is represented by voluminous foreland deposits (Fig. 1b), with Early Cretaceous – early Eocene and early Oligocene – late Miocene siliciclastic sequences (e.g. Faupl and Wagreich, 1992; Kempf et al., 1999).

2.2.3. Carpathians

The Carpathian arc can be geographically subdivided into Western-, Eastern-, and Southern Carpathians (Fig. 1a). Structurally, it consists of the Inner Carpathians and a foreland basin (i.e. Outer Carpathians) with an oceanic suture (i.e. Klippen Belt) zone in-between (e.g. Săndulescu et al., 1981; Nemčok et al., 1998; Krobicki et al., 2003; Fig. 1b).

The major nappes of the Inner Carpathians comprise a dominantly Neoproterozoic – Early Paleozoic basement, covered by late Paleozoic – Mesozoic sedimentary sequences (e.g. Săndulescu et al., 1981; Kováč et al., 1994; Plašienka et al., 1997; Fig. 1b). Basement units are mainly amphibolite facies rocks (Fig. 2a), metamorphosed during the Caledonian and the Variscan orogenies (e.g. Balintoni and Balica, 2013; Stoica et al., 2016). These were intruded by granitoids at various stages during the Paleozoic (e.g. Uher and Broska, 1996; Seghedi et al., 2005; Balintoni and Balica, 2013). Locally, basement rocks experienced a Cretaceous greenschist facies overprint as well (Danišík et al., 2008a; Králiková et al., 2014a). Sedimentary cover sequences of the basement nappes include clastic and carbonatic successions, which were metamorphosed up to greenschist facies conditions in the Cretaceous (e.g. Săndulescu et al., 1981; Bojar et al., 1998; Petrasová et al., 2007). Large areas of the basement are autochtonously covered by (Cretaceous –) Paleogene and Neogene clastic sediments (e.g. Krézsek and Bally, 2006; Fig. 1b). These serve as significant sources of recycled material in the study area (e.g. Schuller and Frisch, 2006; Obbágy et al., 2021). The bedrock pattern of the Inner Carpathians is further complicated by

widespread calc-alkaline volcanics (Fig. 1b, Table S1). They show progressive NW-SE younging (between ca. 16 and 0.03 Ma) along the arc (Pécskay et al., 1995; Lexa et al., 2010; Molnár et al., 2019) and are mainly concentrated in the Western Carpathians. Miocene (between ca. 18 and 14 Ma; Lukács et al., 2018) felsic pyroclastics are also present, mainly distributed along a SW-NE swath in the Western Carpathians.

The Outer Carpathians represent an accretionary wedge comprising a thin-skinned nappe stack of Upper Jurassic to lower Miocene clastic foreland basin sediments (Figs. 1b, 2a) thrust over the Miocene-Quaternary sediments of the European foredeep (e.g. Oszczypko, 2006).

2.2.4. Apuseni Mountains

The Apuseni Mountains represent the surface outcrops of basement nappes found beneath the Pannonian Basin (Fig. 1; e.g. Csontos and Vörös, 2004). The northern Apuseni Mountains comprise a roughly NW-verging Mesozoic stack of three continental basement and/or cover nappe systems (Dallmeyer et al., 1999; Csontos and Vörös, 2004). All three units contain a crystalline basement of Precambrian – Cambrian protolith age, which were metamorphosed at amphibolite facies conditions during Variscan orogeny (e.g. Balintoni et al., 2010) and experienced greenschist facies overprint during the Eoalpine phase (e.g. Reiser et al., 2019). The basement nappes had been intruded by *syn-* to post-Variscan granitoids and transgressively covered by Permian to Lower Cretaceous carbonates and siliciclastic sediments (Pană et al., 2002; Balintoni et al., 2010). Further igneous occurrences in the Apuseni Mountains include Late Cretaceous intrusions (e.g. Gallhofer et al., 2015) and Neogene volcanics (Fig. 1b, Table S1). The three nappe systems are unconformably covered by late Albian to Cenomanian clastic sediments and by Turonian to Maastrichtian "Gosau-type" sediments (e.g. Schuller et al., 2009). The previously described units are separated from the Southern Carpathians by Neotethys-related ophiolitic nappes, occupying the largest part of the southern Apuseni Mountains (Nicolae, 1992).

2.3. Available bedrock FT ages of the potential source areas

Bedrock FT data is summarized in Fig. 2b and c as well as in Table S1. The most widespread ZFT ages (Fig. 2b) in the study area are Eoalpine (120–60 Ma), intersected by areas of <20 Ma ZFT ages at tectonic windows in the Eastern Alps (cooling ages/mixed ages) and at Miocene – Quaternary volcanic occurrences (eruption ages) along the Carpathians and Apuseni Mountains. The Bohemian Massif stands out with old, dominantly pre-Mesozoic (>250 Ma) ZFT ages, whereas scattered occurrences of ZFT ages between 250 and 120 Ma are found throughout the study area. Available bedrock AFT ages show a more complete areal coverage than ZFT ages but they cover a much smaller age range (Fig. 2c). Areas with young (<20 Ma) AFT ages are the most widespread, recording exhumation (Alps, Carpathians) and volcanic activity (Carpathians, Apuseni Mts.) as well. Older AFT ages are found throughout the study area, but they are dominant in the Bohemian Massif, the Inner Western Carpathians, the Apuseni Mts. and the foreland basin (Fig. 2c). Detailed descriptions of potential source areas with respect to FT ages can be found in Electronic Appendix 1.

3. Samples, methods and data evaluation

Modern river sand samples (Table 1) were collected from the main rivers entering the Pannonian Basin, preferentially from locations close to the entry point (Fig. 1). Where unbiased sampling was hindered by hydroelectric dams, material was collected from Quaternary gravel and sand bars. Usually one sample per river was studied. In order to check if the collected samples are representative, a control sample was also taken from the Tisza and Vah rivers and analyzed by means of HMA (Table S2). The Danube2 sample was collected from a Quaternary gravel bar far from the basin entry point (for mimicking mixed basin-fill sediments) in order to check if it returns an intermediate sedimentary signature between individual rivers' samples.

Approximately 5–7 kg of clastic material was collected from each sampling site. According to laser particle sizer measurements, the sample material was dominated by medium (250–500 μm) to coarse (500–1000 μm) sand, underlining the comparability of individual samples. In order to minimize sampling bias, we sampled (and mixed) several sand bars at each site, usually covering ca. 100 m of horizontal and 10 m of vertical distance.

Most rivers cross state borders and have different names in local languages. In order to avoid confusion, in this study we give preference to the nomenclature applied along the longest course of each river. The Danube represents an exception in this respect due to its well-established name in English.

3.1. Zircon and apatite fission-track analysis

Samples for ZFT and AFT analysis were prepared from the 63–125 μm fraction and further concentrated by a Frantz magnetic separator. Samples were bulk-embedded, meaning that no further treatment or handpicking was applied in order to avoid fractionation or operator bias. In addition to track counting, the shape of crystals (euhedral/anhedral) was registered systematically. This information was used as an additional constraint in catchments that covered both Miocene volcanic fields and areas with Miocene cooling ages. For zircon and apatite fission-track analysis the external detector method was applied (Gleadow, 1981). Fission tracks were counted (Table 2) by R.A. in the newly established fission-track laboratory at the Institute for Nuclear Research of Hungary by an Olympus BX53 microscope equipped with a microscope-computer-controlled stage system (Dumitru, 1993). Personal zeta values were 289.8 ± 4.9 and 116.7 ± 2.2 for apatite and zircon, respectively.

3.2. Heavy mineral analysis

For Raman analysis of heavy minerals (see e.g. Andò and Garzanti, 2014; Lünsdorf et al., 2019), heavy mineral concentrates (63–125 μm fraction) were embedded into epoxy resin and cylindrical mounts of 25 mm diameter were prepared. The mounts were ground and polished in the same manner as the FT samples. Raman spectroscopy measurements were performed at the University of Göttingen by a Horiba Jobin Yvon XploRA Plus spectrometer equipped with an Olympus BX41 microscope, a 532 nm diode laser and a motorised x-y-z stage.

3.3. Fine gravel petrography (FGP)

Where available, the 1.5–2.5 mm fraction obtained by custom made sieves was processed for petrography. For simplicity, the method is

Table 1
Sample localities.

Sample Nr.	Locality		Sample description
	Latitude	Longitude	
Drava	46.607489	14.982370	Terasse, gravel pit
Mur	46.946569	15.506110	Gravel pit
Danube7	48.111668	16.746363	Sand/gravel bar
Danube2	47.386620	19.009990	Gravel bar
Morava	48.601380	16.934099	Gravel bar
Vah	48.744820	17.857410	Gravel pit
Hron	48.407127	18.645440	Sand/gravel bar
Ipoly	47.889053	18.761845	Riverbed material
Sajó	48.283320	20.443129	Sand/gravel bar
Hornád	48.500538	21.259626	Gravel pit
Bodrog	48.361744	21.688684	Sand bar
Tisza	48.118020	22.821182	Sand/gravel bar
Someş	47.778553	23.009953	Sand/gravel bar
Mureş	46.108303	21.569970	Sand/gravel bar
Crişul Repede	47.044456	22.408997	Gravel pit

Table 2
Results of zircon and apatite fission-track dating. Bold numbers indicate central ages and corresponding 1 σ standard deviation.

Sample Nr.	Zircon									Apatite								
	Counted crystals	Spontaneous		Induced		$P\chi^2$(%)	Disp.	ρ_d	n_d	Central age ± 1σ	Counted crystals	Spontaneous		Induced		$P\chi^2$(%)	Disp.	ρ_d	n_d	Central age ± 1σ
		ρ_s	n_s	ρ_i	n_i							ρ_s	n_s	ρ_i	n_i					
Drava	60	80.909	3237	118.626	4746	0	0.58	17.75	15,832	**81.3 ± 6.6**	81	4.435	910	12.66	2598	0	0.72	6.61	6016	**49.7 ± 4.8**
Mur	74	65.749	2851	94.945	4117	0	0.48	18.95	15,832	**79.8 ± 5.1**	96	9.194	1812	15.627	3080	0	0.49	6.3	6016	**56.8 ± 3.7**
Danube7	60	125.37	3919	154.098	4817	100	0.75	18.52	15,832	**106 ± 10.8**	87	20.225	3338	24.478	4040	0	0.57	6.8	6016	**83.8 ± 6**
Danube2	60	114.163	3838	135.61	4559	–	0.78	16.43	15,832	**151.9 ± 15.7**	47	5.427	773	13.353	1902	0	0.86	7.23	6016	**56.3 ± 7.7**
Morava	85	111.692	5979	75.751	4055	0	0.58	17.58	15,832	**198.7 ± 12.2**	31	23.322	1028	19.919	878	0	0.54	6.86	6016	**125.9 ± 14.4**
Vah	61	119.743	4826	104.384	4207	0	0.62	18.73	15,832	**140.5 ± 12**	89	7.011	1539	19.725	4330	0	0.55	6.55	6016	**35.3 ± 2.5**
Hron	60	39.303	2014	198.175	10,155	0	0.91	17.31	15,832	**22.7 ± 2.8**	98	10.372	2223	19.886	4262	0	0.51	6.92	6016	**56.6 ± 3.7**
Ipoly	60	78.04	3268	161.549	6765	0	0.72	16.76	15,832	**59.6 ± 5.8**	90	7.194	1739	13.262	3206	0	0.56	6.457	6016	**49.5 ± 3.6**
Sajó	41	82.16	1823	110.192	2445	0	0.57	19.5	15,832	**92.5 ± 8.9**	101	16.07	2990	20.267	3771	0	0.34	6.49	6016	**77.7 ± 3.8**
Hornád	100	100.112	5379	121.087	6506	–	0.69	19.66	15,832	**112.3 ± 8.3**	79	10.388	1939	17.615	3288	0	0.63	6.74	6016	**62.6 ± 5.1**
Bodrog	41	113.681	2217	141.575	2761	0	0.83	18.14	15,832	**110.6 ± 14.8**	39	11	771	20.382	1429	0	0.63	6.98	6016	**58.7 ± 6.8**
Tisza	60	106.575	4421	85.084	3530	0	0.58	18.3	15,832	**141.6 ± 11.6**	52	6.94	499	18.88	1358	0	0.77	6.92	6016	**46.4 ± 5.8**
Someş	61	112.066	4109	118.475	4344	0	0.67	19.28	15,832	**122.8 ± 11.1**	85	9.111	1708	13.566	2543	0	0.57	6.37	6016	**63.8 ± 4.8**
Crişul Repede	60	98.302	4474	135.116	6150	0	0.61	20.05	15,832	**101 ± 8.5**	50	8.976	1211	11.051	1491	0	0.39	6.43	6016	**82.6 ± 6.2**
Mureş	60	124.11	3599	130.921	3797	0	0.6	16.98	15,832	**102.8 ± 8.6**	97	8.385	1796	10.152	2175	0	0.35	6.395	6016	**75.8 ± 4.2**

ρ_s, ρ_i = spontaneous and induced track density, n = number of tracks, $P\chi^2$ = chi-squared value, Disp. = dispersion.

referred to as 'fine gravel petrography', although the studied fraction also contained very coarse sand. The applied grain size range is large enough for the identification of rock types, whereas it allows for the description of a statistically robust amount of grains. This approach helps linking different heavy minerals within a sample to certain source rock types. Due to their resistivity, quartzite and gneiss are dominant in almost all samples (Table S2) while carrying little information about provenance. Therefore, quartzite was not included in FGP plot and FGP data were not evaluated quantitatively.

3.4. Statistical dissimilarity measures

The data obtained via the methods described above were treated by the 'provenance' package of Vermeesch et al. (2016) and by the 'factoextra' package (Kassambara, 2017), both running in R. More specifically, special cases of multidimensional scaling, namely correspondence analysis and the so-called individual scaling was applied to our dataset. The choice of methods is largely based on the recommendations made by Vermeesch (2019). Multidimensional scaling is a superset of principal component analysis that can be used for extracting two- (or higher) dimensional information from a higher dimensional dataset, using pairwise distances between objects (e.g. Torgerson, 1952; Vermeesch, 2013). Our dataset includes different kinds of data, such as point-counting (HM) and age data (ZFT and AFT). Dissimilarity measures in the case of the current dataset were based on the Kolmogorov-Smirnov test (K—S test) and Chi-square test for age data and point counting data, respectively. Correspondence analysis was applied to our HM dataset, as it is similar to but better suited for comparing point-counting data including zero values than the more traditional principal component analysis (Vermeesch, 2019). On the other hand, individual scaling is ideal for comparing different types of data – such as our dataset – via different dissimilarity measures and summarizing dissimilarities in one plot.

Further methodological details can be found in Electronic Appendix 2.

4. Results

The following results are summarized in Tables 2–4 as well as in Figs. 3 and 4.

4.1. Bohemian Massif

The detrital ZFT spectrum of the Morava river (Fig. 3a) is dominated by ages around 200 Ma and older. The dominance of the Permo-Triassic ZFT age component (>60%, Table 4) is unique to this river. This is accompanied by a Triassic AFT age component of ~50%. However, the Morava sample contains a low amount of datable apatite grains and AFT ages are more or less evenly scattered between 270 and 60 Ma. The HM assemblage of the Morava river contains mostly metamorphic minerals, such as garnet, parametamorphic minerals (sillimanite, kyanite, staurolite, chloritoid), epidote group minerals (epidote, zoisite, clinozoisite), as well as about 16% ZTR (zircon+turmaline+rutile) and < 1% chromian spinel.

4.2. Eastern Alps

Major rivers draining the Eastern Alps and entering the Pannonian Basin are Drava, Mur and Danube (only part of its catchment). The detrital FT spectrum (Figs. 3a, b) of the Drava river is dominated by 100–50 Ma ZFT (~70%) and 50–20 Ma AFT ages (~80%), respectively (Table 4). Its HM association is characterized by garnet (>30%), epidote group minerals (ca. 20%) and amphibole (ca. 20%), similarly to the HM assemblage of the Mur (Fig. 4a; Table 3). On the other hand, the Mur sample contains abundant (~60%) ZFT ages younger and AFT ages older than 50 Ma (Fig. 3). The proportion of ZTR minerals is around 10% in

Table 3
Results of heavy mineral analysis via Raman-spectroscopy.

in %	Rt	Ant	Brk	Zrn	Tur	Ap	Mnz	Cr-Spl	Grt	Param	Ttn	Ep gr.	Act-Tr	Ed	Hbl	Cpx	Opx	Ol	Other	ZTR	n
Drava	2.6	0.0	0.1	0.1	2.2	9.3	0.0	0.0	35.8	1.9	3.4	22.5	7.4	8.7	4.5	1.0	0.0	0.0	0.4	4.9	732
Mur	3.2	0.0	0.1	0.4	1.4	3.4	0.0	0.0	39.6	4.2	2.2	16.9	6.3	14.0	7.3	0.3	0.1	0.0	0.4	5.0	714
Danube7	7.3	0.3	0.1	1.6	0.8	3.7	0.0	0.0	40.5	4.6	3.1	25.5	5.2	4.6	2.4	0.3	0.0	0.0	0.1	9.7	765
Danube2	4.5	0.0	0.2	1.4	0.9	1.4	0.3	0.3	55.9	6.1	1.6	13.3	3.0	4.7	3.1	0.9	1.4	0.2	0.7	6.8	572
Morava	8.1	0.2	0.7	6.6	1.6	2.6	0.2	0.2	27.3	6.0	2.0	9.2	12.3	14.7	7.1	0.5	0.2	0.0	0.5	16.3	546
Vah	18.3	0.6	1.7	6.4	3.1	8.3	1.4	2.5	39.2	1.6	1.1	6.8	1.2	2.0	1.2	2.2	1.8	0.1	0.5	27.8	649
Hron	1.6	0.2	0.0	0.6	0.0	2.2	0.5	0.0	1.3	0.0	0.3	3.4	0.5	1.0	6.1	18.4	61.6	2.1	0.3	2.2	625
Ipoly	2.4	0.2	0.3	0.8	0.3	1.6	0.2	0.0	22.3	1.5	0.5	2.9	0.8	1.3	7.8	14.8	42.0	0.2	0.2	3.6	615
Sajó	6.3	0.9	0.2	1.3	1.7	5.4	0.0	0.2	32.2	1.1	2.8	24.6	4.4	4.6	2.7	1.7	7.6	1.4	0.8	9.3	633
Hornád	11.7	0.3	1.0	2.5	1.3	4.9	0.0	2.1	14.2	2.2	0.6	1.5	1.2	0.9	1.5	10.7	42.1	0.4	0.9	15.6	675
Bodrog	9.5	0.5	0.9	2.0	0.9	3.1	0.1	1.0	29.2	2.9	0.9	2.8	1.0	1.7	1.9	9.8	30.9	0.1	0.6	12.4	783
Tisza	16.4	2.1	2.0	4.4	1.9	7.6	0.3	0.5	34.9	1.6	0.9	6.1	0.8	1.2	0.7	8.0	10.0	0.0	0.4	22.7	748
Someş	8.0	0.0	0.3	1.9	1.7	2.4	0.0	1.2	28.4	4.2	1.7	3.4	2.9	4.1	5.3	8.8	25.0	0.3	0.5	11.5	589
Crişul	9.9	3.1	0.2	4.9	2.6	3.1	1.2	0.5	46.9	8.4	3.9	8.1	2.0	1.8	2.5	0.2	0.3	0.0	0.5	17.4	608
Mureş	7.0	0.3	0.2	1.8	1.2	3.2	0.0	0.0	24.8	4.2	2.8	18.0	5.3	5.7	7.2	6.2	11.8	0.3	0.0	10.0	600

Rt = rutile, Ant = anatase, Brk = brookite, Zrn = zircon, Tur = tourmaline, Ap = apatite, Mnz = monazite, Cr-Spl = chromian spinel, Grt = garnet, Param = sillimanite, kyanite, staurolite, chloritoid, Ttn = titanite, Ep gr. = epidote group, clinozoisite, zoisite, Act-Tr = actinolite-tremolite, Ed = edenite, Hbl = other amphibole, mainly hornblende, Cpx = clinopyroxene, Opx = orthopyroxene, Ol = olivine.

the Danube river (Danube7) sample, roughly the double of of their abundance in Drava and Mur (Table 3). Besides abundant AFT (~50%) and ZFT ages (~45%) between 100 and 50 Ma, the Danube7 sample is also characterized by a Jurassic AFT and a Permo-Triassic ZFT age component (Table 4).

4.3. Western Carpathians

The ZFT spectrum of the Vah sample shows a broad scatter of ages between Paleozoic and Paleogene (Fig. 3a) and a restricted set of AFT ages between 100 and 5 Ma (Fig. 3b). These ages are accompanied by a low amount of amphibole (ca. 4%; Table 3) but abundant ZTR (28%) and chromian spinel (>2%). Among the fine gravels (Fig. 4b) granitic and sedimentary/metasedimentary constituents dominate.

ZFT ages in the Hron river sample contain ages almost exclusively (~90%) between 20 and 10 Ma (Fig. 3a) whereas its AFT age distribution (Fig. 3b) is dominated by Late Cretaceous-Paleogene ages. Heavy mineral and fine gravel data suggest extreme dominance of volcanic constituents (e.g. ~80% pyroxene, Fig. 4a).

The Ipoly river sample also comprises abundant ZFT ages between 20 and 10 Ma (~30%), but it is dominated by ages between 100 and 50 Ma (~50%; Fig. 3a). Among AFT ages the Paleogene (45%, Table 4) and the Late Cretaceous (28%) age components are the most dominant. Both the ZFT and the AFT spectrum includes scattered, but noticeable ages between 250 and 100 Ma as well. Its HM and FG composition is similar to the Hron sample, however, the dominantly volcanic signal (>50% pyroxene) is diluted by over 20% garnet and other metamorphic constituents (Fig. 4).

ZFT and AFT ages of the Sajó river can be grouped into Paleogene (~10%), Late-Cretaceous (~55%) and Jurassic (~35%) age components (Table 4). The HM association is dominated by mainly metamorphic constituents, such as garnet (>30%) and epidote group minerals (>20%), whereas the most abundant lithologies among fine gravels are phyllite, micaschist, granite and metasandstone (Fig. 4b).

The Hornád sample shows widespread ZFT ages with Miocene (~10%), Late Cretaceous–Paleogene (~20%) and Early Cretaceous (~30%) ZFT and AFT (30%, 40%, 30%, respectively) components as well as a Jurassic ZFT component (~30%; Table 4.). Among HM-s pyroxenes are the most abundant (>50%), but garnet and ZTR are also present in more than 15% (Table 3). Fine gravels are evenly distributed between the magmatic, sedimentary and metamorphic group. The metamorphic group is represented by abundant mylonitic gravels, a unique feature in this sample (Fig. 4b).

The Bodrog river sample contains few datable zircon and apatite grains. ZFT ages are evenly scattered with no clearly detectable age components, whereas AFT ages are <110 Ma (>80%) with an apparent maximum between 40 and 30 Ma (Fig. 3). Importantly, all ZFT and AFT ages between 20 and 10 Ma were obtained from euhedral grains. The HM spectrum of this sample is a balanced mixture of volcanic (e.g. pyroxenes: 40%), ultrastable (ZTR: 12%) and metamorphic (e.g. garnet: 29%) minerals.

In summary, the Western Carpathians shed a broad range of ZFT ages to the Pannonian Basin with abundant Miocene, Cretaceous (Eoalpine and pre-Eoalpine) and Variscan to Jurassic ages (Fig. 5a). These are accompanied by dominantly Paleogene and Cretaceous AFT dates (Fig. 5b). Heavy mineral and fine gravel compositions carry evidence for input from volcanic, metamorphic and recycled sedimentary sources, the volcanic component being dominant except for the Vah and the small Sajó catchment.

4.4. Eastern Carpathians

The Eastern Carpathians include the entire Tisza and the largest part of the Someş catchment (Fig. 1). ZFT ages in the Tisza sample (Fig. 3a) are evenly spread with no clearly definable age components (Fig. 3a). On the other hand, AFT ages are concentrated between 70 and 10 Ma with a

Table 4
Results of zircon and apatite fission-track age component identification using Binomfit software (Brandon, 2002).

	M1	SD1	SD1	Frac.	M2	SD2	SD2	Frac.	M3	SD3	SD3	Frac.	M4	SD4	SD4	Frac.
ZFT age components																
Drava	16.8	−2.4	2.8	9.7	70.9	−5.2	5.7	67.6	191.7	−25.9	29.8	22.6				
Mur	33.0	−6.5	8.2	14.9	75.8	−7.1	7.8	67.8	186.8	−30.1	35.7	17.3				
Danube7	19.9	−2.4	2.7	14.6	78.3	−5.9	6.4	44.0	235.4	−19.7	21.4	41.4				
Danube2	16.1	−1.8	2.0	15.2	85.8	−8.5	9.5	32.9	203.2	−17.2	18.7	51.8				
Morava	36.3	−5.3	6.2	7.4	96.0	−9.4	10.4	28.2	240.0	−17.3	18.6	64.4				
Vah	41.3	−5.3	6.1	12.0	110.1	−8.1	8.8	50.6	303.5	−28.2	31.0	37.4				
Hron	15.2	−1.0	1.1	87.0	111.6	−14.3	16.4	13.0								
Ipoly	19.2	−1.6	1.8	31.3	68.5	−5.6	6.1	47.1	157.2	−18.6	21.1	21.7				
Sajó	27.4	−5.5	6.9	10.1	73.0	−6.9	7.6	54.3	172.8	−23.3	26.9	35.6				
Hornád	20.0	−2.3	2.6	10.0	62.3	−9.7	11.4	19.7	105.1	−19.0	23.1	29.9	190.3	−26.0	30.0	27.4
Bodrog	25.7	−3.5	4.0	19.7	73.4	−8.7	9.9	30.0	243.4	−26.4	29.5	50.3				
Tisza	29.0	−6.0	7.5	5.1	77.0	−8.1	9.1	23.2	146.1	−15.7	17.6	41.4	285.6	−35.9	41.0	30.3
Someş	14.3	−2.3	2.8	6.6	94.6	−7.1	7.7	52.8	189.5	−25.7	29.7	28.1				
Crişul Repede	23.8	−2.7	3.0	13.2	90.0	−6.0	6.4	58.4	217.3	−23.0	25.6	28.4				
Mureş	23.7	−3.6	4.2	11.6	88.5	−7.1	7.7	55.3	206.5	−20.2	22.4	33.0				
AFT age components																
Drava	2.4	−0.9	1.4	2.5	34.3	−3.5	3.9	80.8	246.6	−66.2	89.9	16.7				
Mur	17.8	−3.4	4.2	16.1	44.7	−12.2	16.8	25.5	77.9	−11.4	13.4	58.5				
Danube7	17.6	−3.6	4.6	11.5	70.3	−5.8	6.4	52.8	157.1	−15.5	17.2	35.8				
Danube2	17.3	−2.5	3.0	40.9	157.7	−30.5	37.7	25.1	69.3	−12.2	14.7	34.1				
Morava	12.4	−5.2	8.9	3.2	91.4	−15.4	18.5	49.0	198.3	−43.4	55.4	47.7				
Vah	15.5	−2.3	2.7	30.7	36.8	−5.2	6.1	46.2	63.9	−14.1	18.1	21.2	198.6	−84.5	145.4	1.9
Hron	9.4	−5.3	12.1	2.6	32.8	−3.6	4.0	34.1	62.3	−7.4	8.4	45.1	119.8	−21.1	25.6	18.2
Ipoly	14.1	−4.0	5.5	16.3	41.4	−5.9	6.9	45.0	77.9	−16.7	21.2	28.2	116.6	−43.6	69.2	10.5
Sajó	49.9	−6.8	7.9	29.2	83.9	−9.8	11.1	60.1	173.6	−49.4	68.7	10.7				
Hornád	25.9	−4.3	5.1	31.5	59.1	−11.8	14.7	37.3	135.0	−22.7	27.3	31.2				
Bodrog	12.7	−4.3	6.6	14.0	47.1	−7.3	8.7	45.7	106.2	−18.0	21.6	40.3				
Tisza	17.2	−3.0	3.7	44.7	50.5	−13.3	17.9	25.5	124.7	−29.5	38.6	29.8				
Someş	18.7	−4.9	6.5	11.4	55.0	−5.6	6.3	65.2	162.2	−25.4	30.0	23.4				
Crişul Repede	66.9	−7.0	7.8	85.4	195.8	−94.1	178.8	14.6								
Mureş	10.5	−8.1	35.5	1.4	48.6	−11.3	14.8	25.6	81.3	−11.2	13.0	65.8	167.8	−48.7	68.2	7.3

M = Mean, SD = standard deviation, Frac. = percentage of detrital ages included in the actual age component.

20–10 Ma maximum and show a strong negative skewness (Fig. 3b). In order to unravel the source of Miocene ages (magmatic or cooling ages), shapes of young (<25 Ma) apatite grains were thoroughly investigated under microscope. Accordingly, the sample contains only rounded young apatite crystals, euhedral apatite grains being completely absent. Furthermore, this sample shows a high ZTR content (23%), whereas pyroxene (~20%) and chromian spinel (0.5%) are also present (Fig. 4a). The fine gravel spectrum shows sandstone dominance and felsic volcanic contribution (Fig. 4b).

Dominant age components in the Someş sample are around 100 Ma for ZFT (~50%) and 50 Ma for AFT ages (~65%), respectively (Fig. 3, Table 4). Further ZFT and AFT age components include Jurassic and Miocene ones. Heavy mineral and fine gravel compositions show a mixed composition (Fig. 4). Heavy minerals are dominated by over 30% pyroxene, somewhat less garnet and around 10% ZTR.

In summary, the "Eastern Carpathian" signal can be distinguished from the signatures of the other four source areas by the following characteristics: (i) volcanic heavy minerals form a significant component but are less dominant compared to the Western Carpathians, (ii) high ZTR and sedimentary gravel content (especially in the Tisza catchment) (iii) abundant young (<20 Ma) rounded apatite crystals (iv) early Late Cretaceous ZFT age maximum at around 100–90 Ma (Fig. 5).

4.5. Southern Carpathians/Apuseni Mts

Although the catchment of the Crişul Repede is restricted to the Apuseni Mts., whereas the Mureş also samples the Eastern and Southern Carpathians, the two rivers are included in one group here for simplicity. The catchment of the Crişul Repede represents only a small part of the study area (Fig. 1b). Its ZFT and AFT spectra show a maximum around 100 Ma and abundant ages between 100 and 50 Ma (ZFT: ~60%; AFT: 85%; Fig. 3). A further, Jurassic component appears in both spectra (Table 4). The HM composition is dominated by over 40% garnet, but the ZTR content (17%) is also significant (Fig. 4a, Table 3). This sample shows the second highest felsic/intermediate igneous gravel content after the Hron (Fig. 4b).

The Mureş drains a wide range of geological formations from the Apuseni Mts., the Eastern Carpathians and the Southern Carpathians. ZFT data can be described by a Miocene (12%), a Late Cretaceous (55%) and a Late Triassic/Early Jurassic age component (33%, Table 4). It is remarkable that the ophiolitic occurrences in the Mureş catchment are clearly detectable by FGP (Fig. 4b), but chromian spinel is completely absent from the heavy mineral spectrum (Fig. 4a).

In summary, the provenance signature of the Southern Carpathians/Apuseni Mts. is dominated by ZFT and AFT ages between 120 and 50 Ma (Fig. 5) and a heavy mineral spectrum with low volcanic contribution (as compared to Eastern and Western Carpathians).

5. Discussion

5.1. Role of recycling

In order to evaluate the agreement between detrital signatures and available bedrock data, the effect of possible recycling has to be considered. In the study area, Cretaceous – Miocene foreland basin sediments, Paleogene sediments and Neogene sediments can act as sources for recycled material. We calculated the areal distribution of the three sedimentary basin types in each catchment (Table 5). Combined with our provenance dataset this allows for estimating their relative contribution to recycling. Notably, we did not quantify various factors (e.g. fertility, diagenesis, topography) in this study that could potentially also influence our results (e.g. Morton and Hallsworth, 1999; Caracciolo, 2020).

The ZTR index (Huber, 1962) is the most common indicator of recycling, however, it can be significantly biased by igneous and metamorphic bedrock characterized by high fertility with respect to

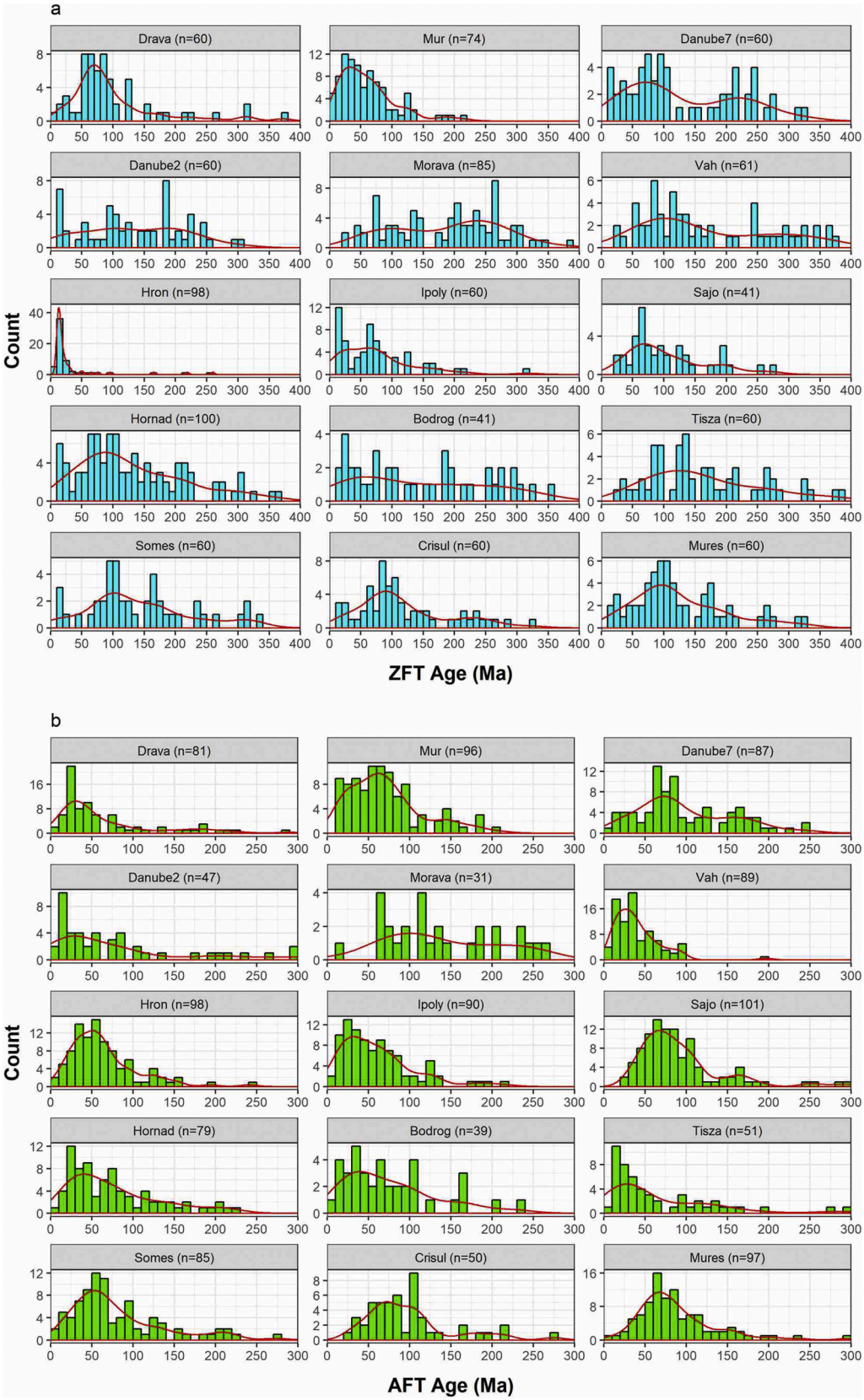

Fig. 3. Detrital zircon (a) and apatite (b) fission-track age distributions of individual rivers with the number of dated grains (in brackets) and probability density distributions (red lines). Note the different x and y scales for ZFT and AFT data. (For interpretation of the references to colour in this figure legend, the reader is referred to the web version of this article.)

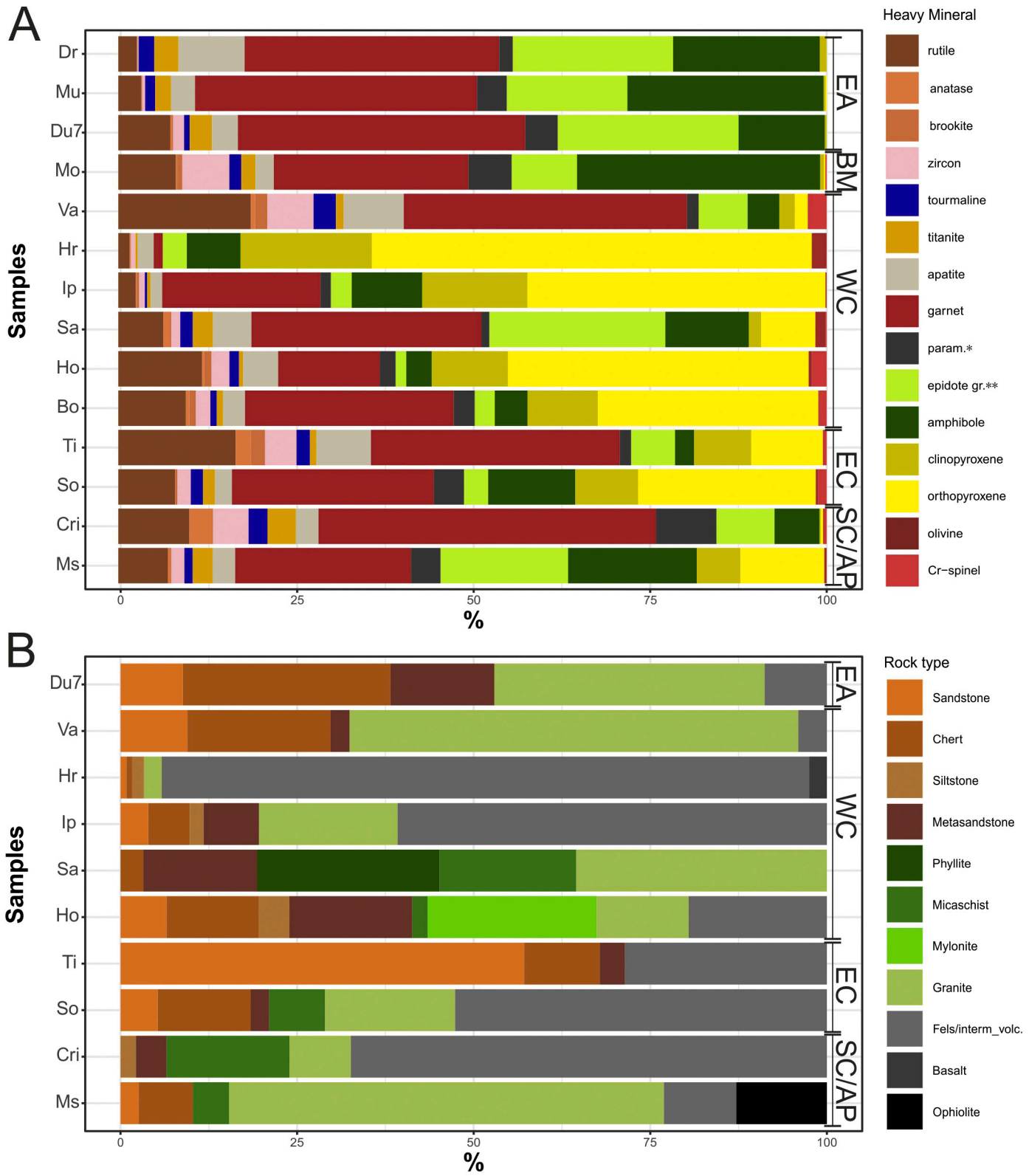

Fig. 4. Heavy mineral (a) and fine gravel (b) compositions of individual river samples grouped according to potential souce areas. *rutile, anatase, brookite **sillimanite, kyanite, staurolite, chloritoid ***epidote, zoisite, clinozoisite; Param = sillimanite, kyanite, staurolite, chloritoid. EA = Eastern Alps, WC=Western Carpathians, EC = Eastern Carpathians, SC=Southern Carpathians, AP = Apuseni Mts. Sample abbreviations as in Fig. 1b.

zircon, tourmaline and rutile. Possible sources of ultrastable minerals in our study area besides sediments include widespread Neoproterozoic-Early Paleozoic basement rocks and Miocene volcanics as well as Cretaceous igneous rocks of local importance. Fig. 6a shows the correlation matrix between common heavy mineral indices and the areal extent (in %) of different bedrock types in individual catchments. These indices include ZTR, ATi (100*apatite/apatite+tourmaline), GZi (100*garnet/garnet+zircon), RZi (100*rutile/rutile+zircon) and CZi

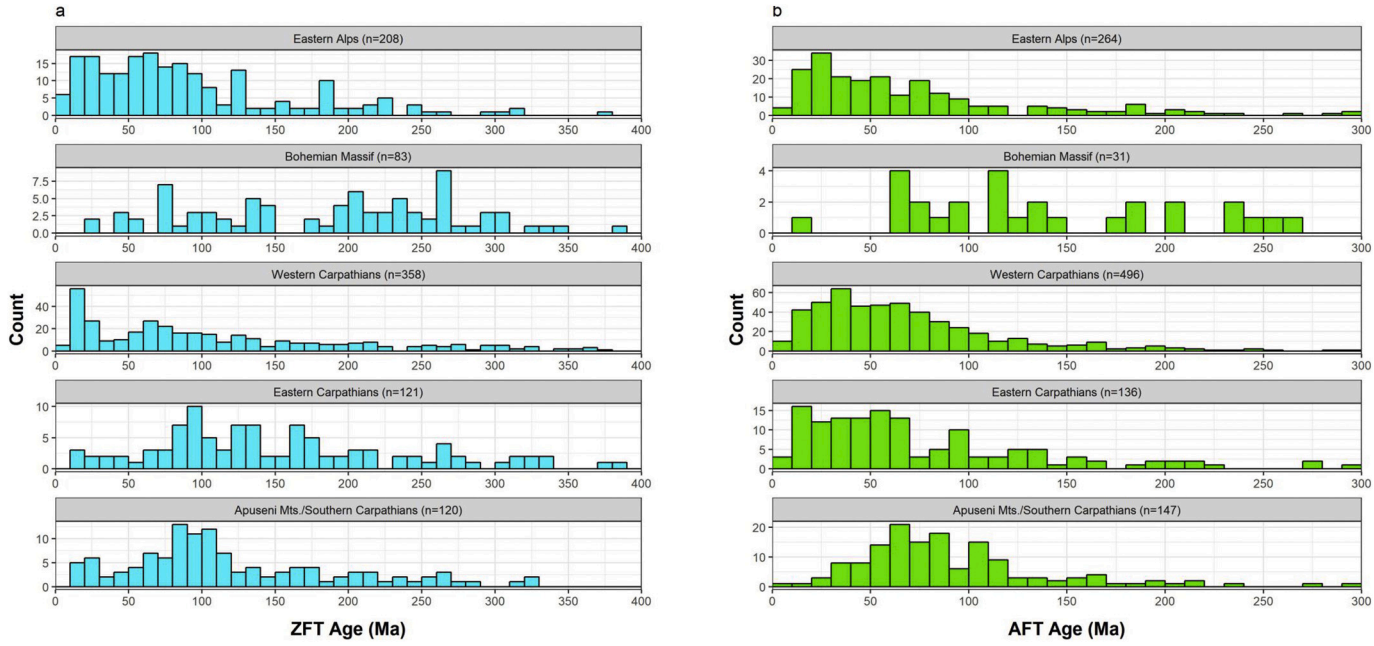

Fig. 5. Summary of zircon (a) and apatite (b) fission-track data according to potential source areas. Note the varying x and y axes.

Table 5
Areal distribution of bedrock lithologies in individual catchments calculated by the ArcGIS software.

in %	Drava	Mur	Danube	Morava	Vah	Hron	Ipoly	Sajó	Hornád	Bodrog	Tisza	Someş	Crişul	Mureş
Neogene sediments	0	6	40	24	4	0	29	11	26	26	0	42	3	49
Neogene volcanics	0	0	0	0	1	43	41	3	7	19	6	6	0	13
Paleogene sediments	0	0	0	0	12	0	18	24	1	4	36	41	17	1
Cretaceous-Miocene Foreland basin	0	0	7	21	33	0	0	0	6	49	45	0	0	0
Jurassic-Cretaceous ophiolite	0	0	0	0	0	0	0	0	0	0	0	0	0	3
Cretaceous Intrusions	0	0	0	0	0	0	0	0	0	0	0	0	30	0
Late Paleozoic-Mesozoic carbonates	12	13	26	4	40	21	0	20	14	2	3	1	16	12
Neoproterozoic-Early Paleozoic metamorphic basement		80	27	52	10	35	12	42	45	1	10	10	34	22
SUM	100	100	100	100	100	100	100	100	100	100	100	100	100	100
SUM (km^2)	11,821	6563	102,705	24,007	10,037	3781	5247	3369	2899	13,146	9437	14,706	1601	26,515

(100*chromian spinel/chromian spinel+zircon; Morton and Hallsworth, 1994). In order to estimate metamorphic contribution via heavy mineral ratios, we also included the Ky/Ky + ZTR ratio (100*kyanite/kyanite+zircon+tourmaline+rutile) in the correlation matrix. Notably, this ratio is not a universally applicable heavy mineral index, as the included components have different hydraulic behavior and stability (Morton and Hallsworth, 1999).

ZTR shows strong positive correlation only with the areal extent of Cretaceous–Miocene foreland sediments and slightly positive correlation with that of Paleogene sediments in individual catchments. In contrast, ZTR does not correlate positively with the coverage of Neoproterozoic-Early Paleozoic basement rocks, Neogene sediments and Neogene volcanics. Thus, the value of ZTR in individual catchments reflects sedimentary recycling, especially through the foreland basin and to a lesser extent through Paleogene sediments. On the other hand, the Ky/Ky + ZTR ratio shows positive correlation only with the areal abundance Neoproterozoic-Early Paleozoic basement rocks, whereas ATi correlates positively with that of Miocene volcanics. A correspondence analysis plot between the above variables (Fig. 6b) provides additional explanation to the correlation matrix. Based on the position of individual rivers in the plot, it can be visually assessed, to which extent is each rivers' detrital HM signal affected by recycling. Accordingly, the samples Tisza, Vah and Bodrog are strongly recycled, whereas the HM signal of Drava, Mur (dominantly metamorphic HM) as well as the Ipoly and Hron (dominantly volcanic HM) show the least signs of recycling.

5.2. Role of fertility

According to Malusá et al. (2016), apatite and zircon mineral fertility values of different lithologies in the Alps may span over three orders of magnitude. Although we did not follow such a quantitative approach as the authors of that study, we can observe fertility bias in one sample. The ZFT age distribution of the Hron sample comprises almost exclusively Miocene ages, in accordance with the dominance of Miocene volcanics in its catchment. Contrastingly, its AFT age distribution (Fig. 3b) is dominated by Late Cretaceous-Paleogene ages, representing the known cooling ages from the basement blocks in the catchment (Fig. 2c). This extreme discrepancy between the AFT and ZFT data suggests that Miocene volcanics in this region are not fertile with respect to apatite, whereas the basement units barely contribute to the zircon content.

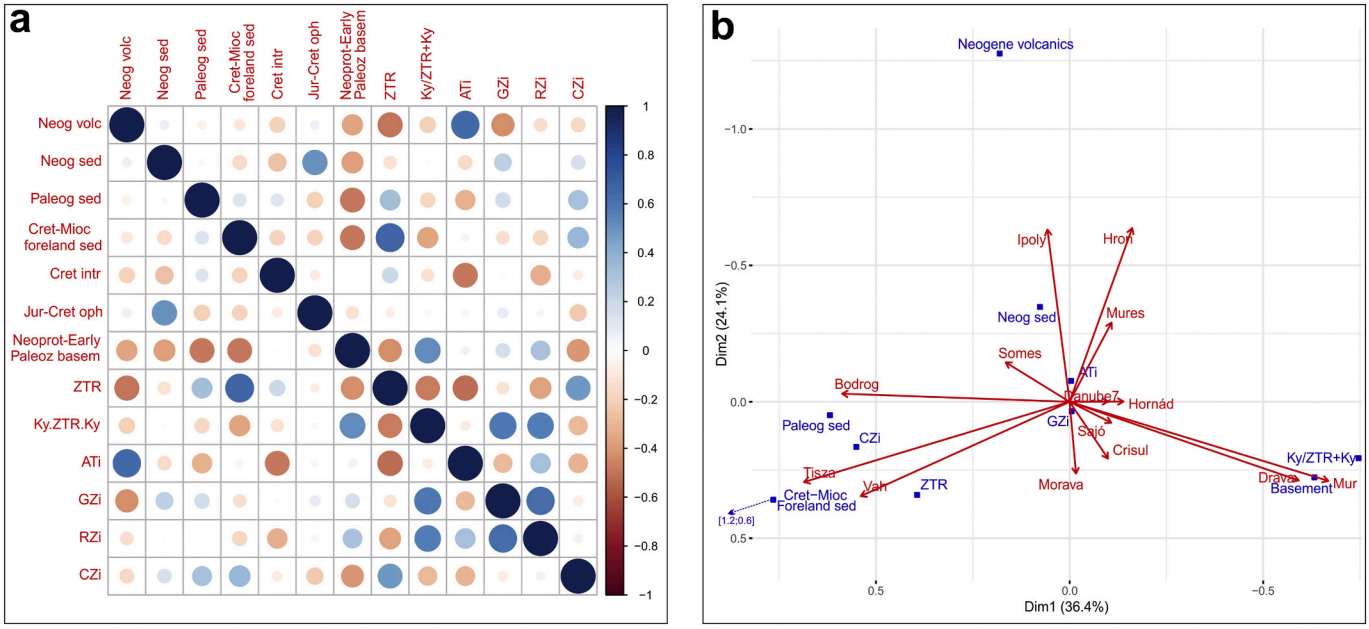

Fig. 6. (a) Correlation matrix between bedrock types and heavy mineral indices. Blue and red colors mark positive and negative correlation coefficients, respectively. Larger spot sizes and darker colors indicate stronger correlation between variables. (b) Correspondence analysis plot based on bedrock areal extents within catchments and heavy mineral indices. Rivers occupy positions according to their characteristic heavy mineral signature. Samples strongly affected by recycling plot lower left. (For interpretation of the references to colour in this figure legend, the reader is referred to the web version of this article.)

5.3. Linking source areas to detrital signatures in individual catchment areas

5.3.1. Bohemian Massif

AFT and ZFT ages in the Morava sample (Fig. 3a) largely overlap with reported bedrock data in the Bohemian Massif (Hejl et al., 1997; Botor et al., 2017), in accordance with its areal dominance in the catchment (>50%, Table 5). Further contribution by recycled sediments is supported by the high ZTR index (~16%) and the occurrence of chromian spinel (Fig. 4a), but a significant foreland basin contribution is unlikely as AFT ages below 50 Ma are common in the foreland basin (e.g. Andreucci et al., 2013, Fig. 2c) but very rare (n = 1) in our sample (Fig. 3b). The dominance of the Bohemian Massif is further supported by the lower proportion of chromian spinel and ZTR in the Morava river sample as compared to the Vah (see below).

In summary, the Morava river sample largely represents the provenance signature of the Bohemian Massif, however, sedimentary recycling is also detectable through the foreland basin (Fig. 6).

5.3.2. Eastern Alps

Paleozoic to Miocene ZFT and Paleogene to Miocene AFT ages as well as dominantly metamorphic lithologies (>80%; Table 5) in the Drava and Mur rivers' catchments (Figs. 1b, 2a, b) are well reflected in the detrital age distributions and the HM spectra. Especially ZFT data from the Drava (Fig. 3a) imply that its detrital signal is dominated by the Eastern Alps, while the erosional products of the Southern Alps are underrepresented. Considering also the bedrock composition within the catchment areas of the Drava and Mur (Table 5), their detrital signature can be considered as a primary fingerprint of the Eastern Alps.

Higher (~10%) ZTR content of the Danube7 sample (Fig. 4a, Table 3) compared to Mur and Drava together with abundant chert and sandstone gravels (Fig. 4b) implies recycling in the foreland basin. However, the extent of recycling in this catchment is considered to be minor (Fig. 6b). Considering ZFT ages older than 150 Ma some/most pre-Eoalpine ages are also provided by the Bohemian Massif. Therefore, the Danube sample can be considered as an Alpine signal with minor Bohemian contribution.

5.3.3. Western Carpathians

Bedrock ages of areally restricted (10%; Table 5) crystalline massifs in the Vah catchment (Fig. 2b and c) alone cover the observed detrital ZFT and AFT age spectrum. However, if we take into account the high proportion of ultrastable minerals, the appearance of chromian spinel and sedimentary/metasedimentary gravels (Fig. 4), the contribution of foreland basin sediments is obvious (e.g. Winkler and Slaczka, 1992, Fig. 6b). This is in accordance with the high (>30%) areal occupancy of the foreland basin within its catchment (Table 5).

The catchments of the Hron, Ipoly, Sajó and Hornád rivers are dominated by Miocene volcanics and crystalline basement to a different extent (Table 5). Modern river sediments generally reproduce bedrock geology and FT age distribution well. Differences compared to bedrock are caused by fertility bias (see Section 5.2) in the Hron river sample and recycling in the Sajó and Hornád. Recycling is evidenced by elevated ZTR indices, the appearance of metasandstone gravels and chromian spinel as well as AFT and ZFT ages older than 100 Ma and 150 Ma, respectively. Candidates for recycling in the Sajó and Hornád catchments include the partly clastic basement cover sequences (not treated quantitatively due to local importance), the foreland basin sediments and the widespread Paleogene sediments, respectively (see Section 5.1).

Miocene AFT and ZFT ages obtained from clearly euhedral grains and the high proportion of pyroxene (Figs. 3 and 4a) suggest a significant contribution by Miocene volcanics to the Bodrog's detrital assemblage. On the other hand, pre-Miocene ZFT and AFT ages together with the appearance of chromian spinel suggest significant recycling in the foreland basin (Fig. 6b). The absence of clearly definable age components in the FT spectra and the abundance of Paleogene AFT ages can be a result of partial thermal reset affecting the sedimentary formations in the foreland (Hurai et al., 2006).

5.3.4. Eastern Carpathians

The HM record of the Tisza shows several signs of recycling (Fig. 6b), in accordance with the dominantly (>80%) clastic bedrock formations in its catchment (Fig. 1b, Table 5). Exclusively rounded young (<20 Ma) apatite crystals and the negatively skewed AFT age distribution (Fig. 3b) support a significant reset in the foreland basin and minor volcanic

contribution. Evenly spread ZFT ages with no clearly definable age components (Fig. 3a) imply that the temperature of thermal resetting could even affect the ZFT thermochronometer.

Dominantly Eoalpine AFT and ZFT ages (Fig. 3) in the Someş sample probably derive from locally occurring (10% of the catchment) crystalline units within the Apuseni Mts. and Eastern Carpathians (Gröger et al., 2013). The contribution of the Miocene age component is also in agreement with the areal distribution of Miocene volcanics (Tables 4 and 5). Less abundant pre-Eoalpine dates cannot be associated with available bedrock data, suggesting recycling. However, ca. 50% less ZTR as compared to the Tisza catchment shows clearly that recycling is much less efficient in the Paleogene and Neogene basins than in the foreland (see also Section 5.1).

5.3.5. *Southern Carpathians/Apuseni Mts*

The dominance of AFT ages between 90 and 50 Ma (Fig. 3b) as well as ZFT ages between 110 and 60 Ma can be explained by the available bedrock FT data in the Crişul Repede catchment (Fig. 2b and c). Cretaceous felsic magmatic contribution is shown by abundant magmatic (granitic) gravels (Fig. 4b) and by ZFT ages between 70 and 60 Ma (Reiser, 2015), whereas ZFT ages older than ca. 150 Ma are probably of recycled origin from Cretaceous sediments (Schuller et al., 2009).

FT ages in the Mureş catchment (Fig. 3) suggest Neogene volcanics (Apuseni Mts. and Eastern Carpathians) as well as basement units and their cover sequences in the Apuseni Mts. and the Southern Carpathians as possible sources. The clear contribution of ophiolitic gravels to the FGA signature (Fig. 4b) together with the complete absence of chromian spinel is striking. This observation suggests that different lithologies may be selectively represented in certain grain size fractions.

5.4. *Detrital FT age spectra in a regional tectonic framework*

If we consider all samples investigated, we can summarize the age components of individual ZFT and AFT age distributions (Table 4) calculated by the Binomfit software of Brandon (2002). The clustering of ZFT age components reproduces the known regional thermotectonic events and the subsequent cooling with remarkable accuracy (Fig. 7). These are namely the Post-Variscan exhumation, the Permo-Triassic rifting, the Jurassic rifting, the Post-Eoalpine exhumation and the Neogene exhumation and/or the Neogene volcanism. Interestingly, the

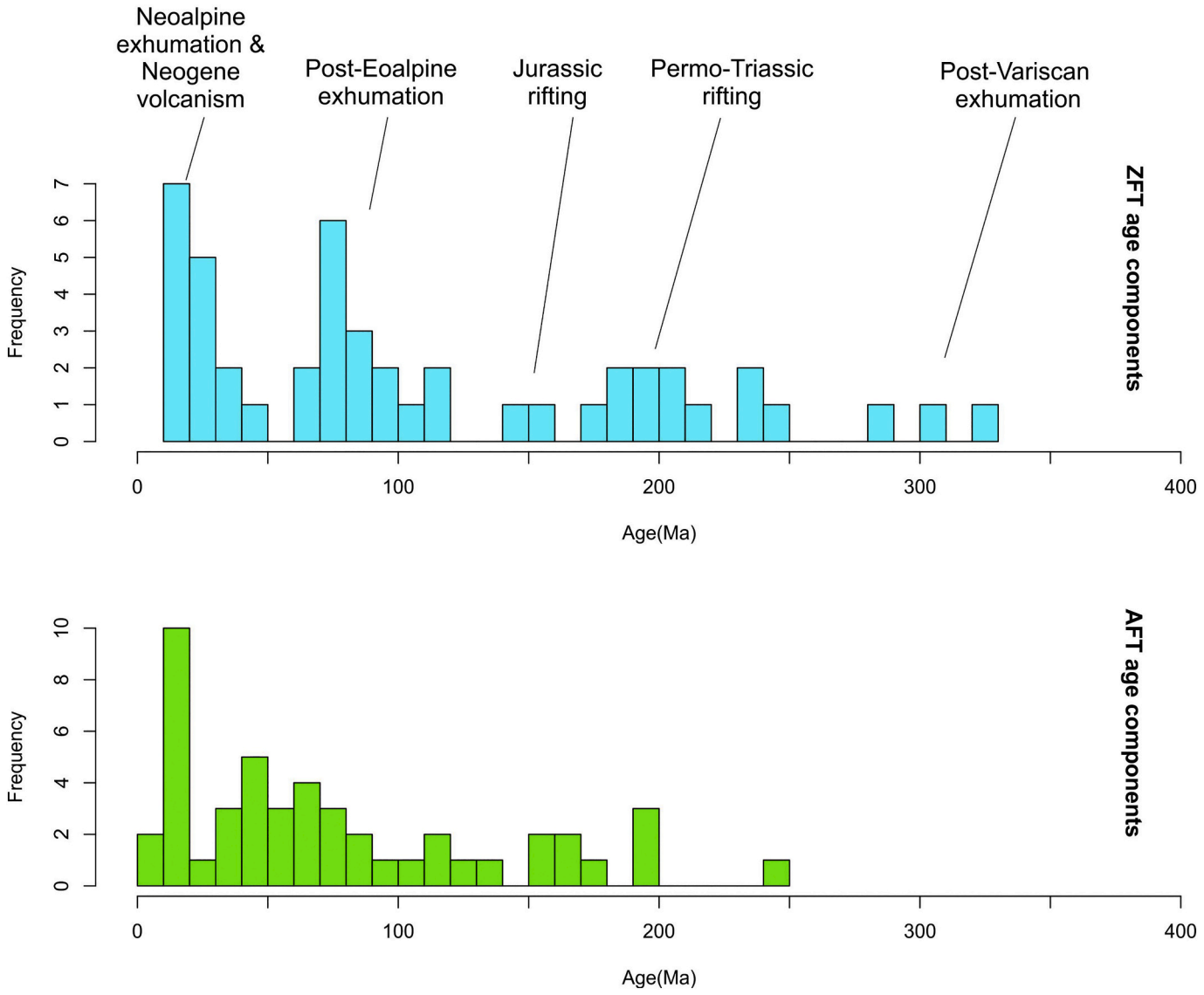

Fig. 7. Compilation of zircon and apatite fission-track age components calculated from individual detrital distributions by the Binomfit software (Brandon, 2002). Note the wider spread of ZFT age components. Major thermotectonic events are highlighted. Note the possible contribution of partially reset ages (Tisza sample) to the Jurassic component. See text for details.

AFT age components fail to reproduce this detailed pattern (Fig. 7). Exceptions include the Miocene and the Eoalpine events, both of which show a younger maximum in frequency than in the case of ZFT components. This can be explained by the lower closure temperature of the AFT system and its higher sensitivity to thermal resetting, often caused by sediment recycling. As a result of this, detrital AFT thermochronology can be considered as a less powerful tool than detrital ZFT thermochronology for tracing sedimentary provenance in regions, where sedimentary recycling is a common phenomenon.

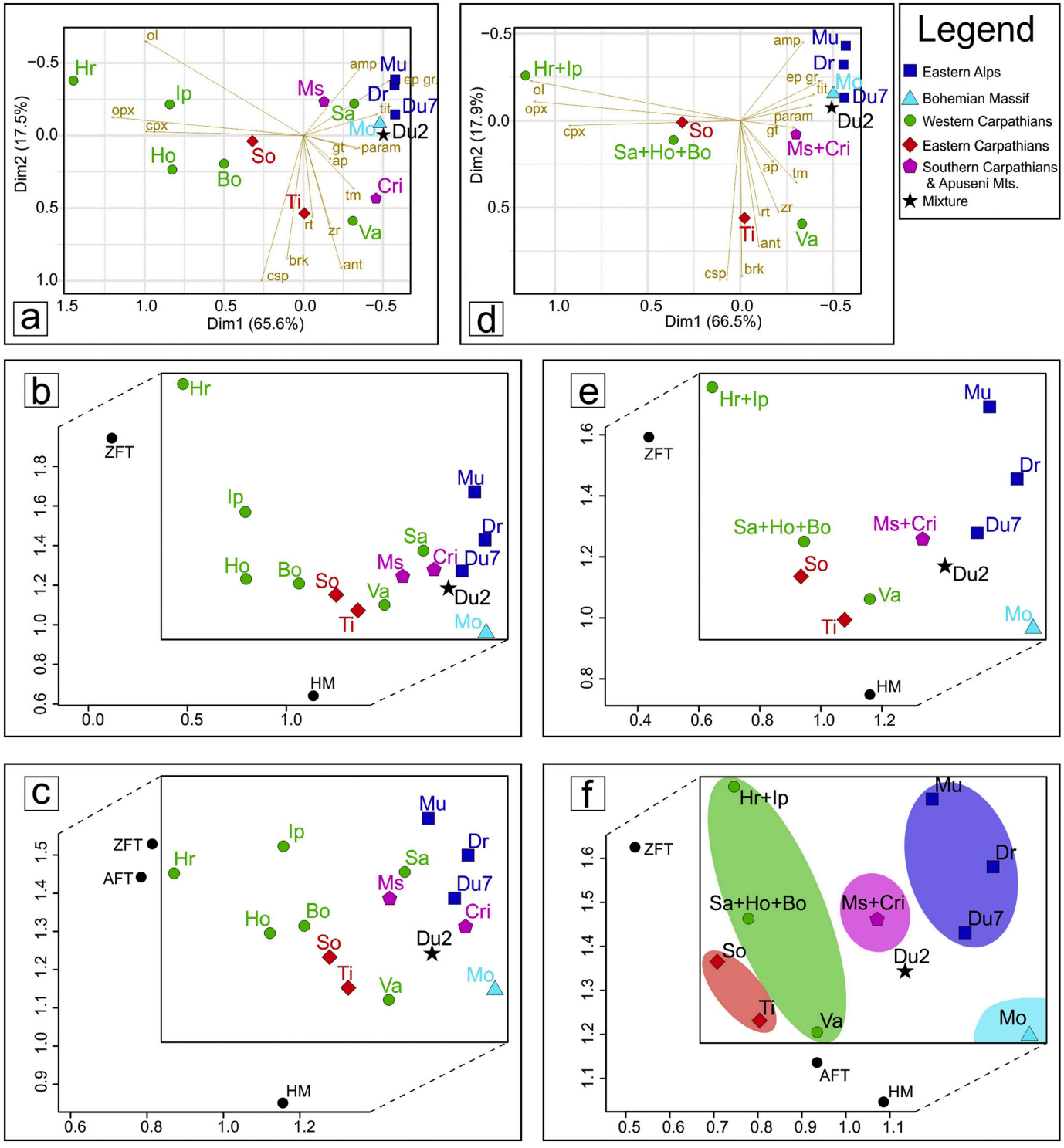

Fig. 8. Results obtained by applying multivariate ordination techniques (Vermeesch, 2016; Kassambara, 2017). Our dataset is shown without (a, b, c) and with (d, e, f) the grouping of smaller rivers to achieve comparable catchment sizes. Correspondence analysis (a, d) shows the contribution of individual heavy minerals/heavy mineral groups to sample discrimination. Plots b and e show the performance of individual scaling algorithm using ZFT and HM as variables. Plots c and f show the performance of individual scaling algorithm using ZFT, AFT and HM as variables. Axes around rectangles explain the influence of individual variables on the x and y axes. Sample abbreviations ar the same as in Fig. 1b. Heavy mineral abbreviations are the same as in Table 2.

5.5. Combined comparison of detrital signatures via statistical dissimilarity measures

The results obtained by applying correspondence analysis and the individual scaling algorithm to our dataset are summarized in Fig. 8. If we include only the HM data to the comparison, correspondence analysis explains differences between individual samples in an intuitive way (Fig. 8a). The relationship between categorical input variables (i.e. heavy mineral type) is shown by vectors and the configuration of the samples can be read from their position within the plot. It is remarkable that the consideration of the HM data alone already results in a geographically logical grouping of individual rivers, showing that detrital HM spectra are largely defined by the potential source areas. The addition of ZFT along with HM data to multidimensional scaling enhances differences between certain samples, but some of them remain almost indistinguishable (Fig. 8b). Here, the x and y axis is defined by the HM content and the ZFT spectrum, respectively (Fig. 8b): samples dominated by young ZFT ages plot higher up, whereas dominantly metamorphic signatures can be found to the right. Adding also AFT data to the comparison, the separation according to potential source area becomes even more visible (Fig. 8c). The ZFT data attaches more weight to the y axis than AFT, which is in line with larger differences between individual ZFT spectra. Despite the logical grouping facilitated by three variables, some discrepancies still exist, such as the apparent similarity of the Sajó, Mureş, Danube, Drava and Crişul Repede data. This is in line with the observations of Thamó-Bozsó and Kovács (2007) who applied principal component analysis to HM data from the same catchments. A possible explanation for the discrepancy is the vast difference between the sizes of individual catchment areas (e.g. Danube vs. Sajó, Table 5), resulting in apparent data similarity on largely different spatial scales. In order to avoid spatial scale bias, adjacent smaller scale rivers were grouped together; groups were treated as individual samples and the 'grouped' dataset was processed in the same way as the original one (Figs. 8d, e and f). Obviously, for such large-scale observations the grouping of smaller adjacent catchments is straightforward as drainage divides in orogenic settings shift through time (e.g., Kuhlemann et al., 2001). Due to the comparison of larger catchments the 'grouped'dataset is less prone to errors related to short-term catchment area changes, which are inherent to our samples of Holocene to Pleistocene stratigraphic age. The resulting dissimilarity diagrams (Figs. 8e, f) show a more clear distinction of individual samples/sample groups. The Eastern Alps are characterized by a high proportion of metamorphic minerals and intermediate (Danube) to young (Mur) ZFT ages as compared to other rivers. The Western Carpathians show a similar spread of ages as the Eastern Alpine rivers but a predominance of volcanic HM (i.e. the two source areas separated via HM, not via FT; Fig. 8f). An exception within Western Carpathians is the Vah catchment, showing a transition towards the Bohemian Massif with respect to FT ages. The Bohemian Massif represents an "endmember" characterized by abundant metamorphic HM and old FT ages. The Eastern Carpathians show a high ratio of volcanic vs. metamorphic HM but intermediate to old ages, whereas the Southern Carpathians/Apuseni Mts. source area is intermediate with respect to all datasets. The Danube2 (Du2) sample also occupies an intermediate position roughly between the Vah and Danube7 samples on the dissimilarity diagram. This renders the future application of the current approach to mixed basin-fill sediments feasible.

6. Conclusions and future perspectives

We compared the sedimentary provenance signatures of modern river samples in the Pannonian Basin by means of zircon and apatite fission-track dating, Raman-spectroscopy-based heavy mineral analysis and fine gravel petrography. The obtained results provide a useful complement to fission-track and heavy mineral datasets in areas where bedrock data is incomplete. Furthermore, detrital data enable to detect the contribution of primary bedrock signatures, differences in mineral fertility and the degree of recycling. Based on HM indices, Cretaceous-Miocene foreland basin sediments and to a lesser extent Paleogene basins are responsible for major recycling, whereas Neogene sedimentary basins do not contribute significantly to this effect. A further major goal of the study was to define distinct sedimentary signatures related to potential source areas in order to explain the origin of large-scale basin-fill sediment mixtures in future studies. The simultaneous application of multiple independent provenance proxies together with statistical dissimilarity measures allows for drawing the following conclusions: (i) Combined provenance signatures in the study area are distinguishable on a river to river and source area to source area basis, (ii) potential source areas occupy distinct fields on dissimilarity plots despite their largely similar geological histories and composition, (iii) large differences in catchment size can result in apparent similarities between individual rivers' detrital signatures, and (iv) spatial-scaling-related bias can be eliminated by grouping smaller, adjacent or related catchments. The clear separation of Eastern Alps, Bohemian Massif, Western Carpathians, Eastern Carpathians and Southern Carpathians/Apuseni Mts. is promising for future 'basin-fill sediment' studies of the following kind: (i) Source area changes in space and/or time across selected sub-basin(s) within the Pannonian Basin related to climatic and/or tectonic variations, (ii) paleogeographic reconstructions based on source-to-sink relationships of well-defined stratigraphic horizons across the entire Pannonian Basin, and (iii) detailed provenance studies along the course of either river in order to quantify the effects of mineral fertility, precipitation, erodibility, topography, etc.. Moreover, the approach is well-suited to be applied in any other (especially large-scale) sedimentary basin system.

Supplementary data to this article can be found online at https://doi.org/10.1016/j.gloplacha.2021.103446.

Declaration of competing interest

There is no conflict of interest related to this manuscript.

Acknowledgements

The research was supported by the PPD2018-003/2018 Premium Postdoctoral Grant of the Hungarian Academy of Sciences as well as the European Union and the State of Hungary, cofinanced by the European Regional Development Fund in the project of GINOP-2.3.2-15-2016-00009 'ICER'. Judit Nagy, Irina Ottenbacher, Zsolt Kertész and Norbert Karacs are thanked for their help in laboratory and manufacturing work. We are grateful for Tamás Weiszburg's help in providing us all essential lab facilities at the Department of Mineralogy, Eötvös Loránd University, Budapest in the first stage of our work and Zsolt Bakonyi's input at fieldwork. Thorough reviews by Edit Thamó-Bozsó, Luca Caracciolo, Andrea Di Giulio, Jocelyn Barbarand and an anonymous reviewer significantly improved the manuscript and are gratefully acknowledged.

References

Anczkiewicz, A.A., Danišík, M., Środoń, J., 2015. Multiple low-temperature thermochronology constraints on exhumation of the Tatra Mountains: new implication for the complex evolution of the Western Carpathians in the Cenozoic. Tectonics 34, 2296–2317.

Andò, S., Garzanti, E., 2014. Raman spectroscopy in heavy-mineral studies. Geol. Soc. Lond., Spec. Publ. 386, 395–412.

Andreucci, B., Castelluccio, A., Jankowski, L., Mazzoli, S., Szaniawski, R., Zattin, M., 2013. Burial and exhumation history of the Polish Outer Carpathians: discriminating the role of thrusting and post-thrusting extension. Tectonophysics 608, 866–883.

Andreucci, B., Castelluccio, A., Corrado, S., Jankowski, L., Mazzoli, S., Szaniawski, R., Zattin, M., 2015. Interplay between the thermal evolution of an orogenic wedge and its retro-wedge basin: An example from the Ukrainian Carpathians. GSA Bulletin 127, 410–427.

Asch, K., 2003. The 1: 5 million international geological map of Europe and adjacent areas: development and implementation of a GIS-enabled concept. BGR., ISBN 3510959035.

Balintoni, I., Balica, C., 2013. Carpathian peri-Gondwanan terranes in the East Carpathians (Romania): a testimony of an Ordovician, North-African orogeny. Gondwana Res. 23, 1053–1070.
Balintoni, I., Balica, C., Ducea, M.N., Zaharia, L., Chen, F., Cliveţi, M., Hann, H., Li, L.-Q., Ghergari, L., 2010. Late Cambrian–Ordovician northeastern Gondwanan terranes in the basement of the Apuseni Mountains, Romania. J. Geol. Soc. 167, 1131–1145.
Balla, Z., 1984. The Carpathian loop and the Pannonian basin: a kinematic analysis. Geophys. Trans. 30, 313–353.
Bertotti, G., Seward, D., Wijbrans, J., Ter Voorde, M., Hurford, A., 1999. Crustal thermal regime prior to, during, and after rifting: a geochronological and modeling study of the Mesozoic South Alpine rifted margin. Tectonics 18, 185–200.
Bojar, A.-V., Neubauer, F., Fritz, H., 1998. Cretaceous to Cenozoic thermal evolution of the southwestern South Carpathians: evidence from fission-track thermochronology. Tectonophysics 297, 229–249.
Botor, D., Dunkl, I., Anczkiewicz, A., Mazur, S., 2017. Post-Variscan thermal history of the Moravo-Silesian lower Carboniferous Culm Basin (NE Czech Republic-SW Poland). Tectonophysics 712, 643–662.
Bousquet, R., Oberhänsli, R., Goffé, B., Wiederkehr, M., Koller, F., Schmid, S.M., Schuster, R., Engi, M., Berger, A., Martinotti, G., 2008. Metamorphism of metasediments at the scale of an orogen: a key to the Tertiary geodynamic evolution of the Alps. Geol. Soc. Lond., Spec. Publ. 298, 393–411.
Brandon, M., 2002. Decomposition of mixed grain age distributions using Binomfit. On Track 24, 13–18.
Burchart, J., 1972. Fission-track age determinations of accessory apatite from the Tatra Mountains, Poland. Earth Planet. Sci. Lett. 15, 418–422.
Caracciolo, L., 2020. Sediment generation and sediment routing systems from a quantitative provenance analysis perspective: Review, application and future development. Earth Sci. Rev. 103226.
Carter, A., 2007. Heavy minerals and detrital fission-track thermochronology. Dev. Sedimentol. 58, 851–868.
Csontos, L., Vörös, A., 2004. Mesozoic plate tectonic reconstruction of the Carpathian region. Palaeogeogr. Palaeoclimatol. Palaeoecol. 210, 1–56.
Dallmeyer, R., Pană, D., Neubauer, F., Erdmer, P., 1999. Tectonothermal evolution of the Apuseni Mountains, Romania: resolution of Variscan versus Alpine events with 40Ar/39Ar ages. J. Geol. 107, 329–352.
Danišík, M., Dunkl, I., Putiš, M., Frisch, W., KráĽ, J., 2004. Tertiary burial and exhumation history of basement highs along the NW margin of the Pannonian Basin – an apatite fission track study. Austrian J. Earth Sci. 95, 60–70.
Danišík, M., Kohut, M., Dunkl, I., Frisch, W., 2008a. Thermal evolution of the Žiar Mountains basement (Inner Western Carpathians, Slovakia) constrained by fission track data. Geol. Carpath. 59, 19–30.
Danišík, M., Kohút, M., Dunkl, I., Hraško, L.u., Frisch, W., 2008b. Apatite fission track and (U-Th)/He thermochronology of the Rochovce granite (Slovakia) – implications for the thermal evolution of the Western Carpathian-Pannonian region. Swiss J. Geosci. 101, 225–233.
Danišík, M., Kohút, M., Broska, I., Frisch, W., 2010. Thermal evolution of the Malá Fatra Mountains (Central Western Carpathians): insights from zircon and apatite fission track thermochronology. Geol. Carpath. 61, 19–27.
Danišík, M., Kadlec, J., Glotzbach, C., Weisheit, A., Dunkl, I., Kohút, M., Evans, N.J., Orvošová, M., McDonald, B.J., 2011. Tracing metamorphism, exhumation and topographic evolution in orogenic belts by multiple thermochronology: a case study from the Nízke Tatry Mts., Western Carpathians. Swiss J. Geosci. 104, 285–298.
Danišík, M., Kohut, M., Evans, N.J., McDonald, B.J., 2012. Eo-Alpine metamorphism and the 'mid-Miocene thermal event' in the Western Carpathians (Slovakia): new evidence from multiple thermochronology. Geol. Mag. 149, 158–171.
Di Giulio, A., Ceriani, A., Ghia, E., Zucca, F., 2003. Composition of modern stream sands derived from sedimentary source rocks in a temperate climate (Northern Apennines, Italy). Sediment. Geol. 158, 145–161.
Dumitru, T.A., 1993. A new computer-automated microscope stage system for fission-track analysis. Nuclear Tracks and Radiation Measurements 21, 575–580.
Dunkl, I., Grasemann, B., Frisch, W., 1998. Thermal effects of exhumation of a metamorphic core complex on hanging wall syn-rift sediments: an example from the Rechnitz Window, Eastern Alps. Tectonophysics 297, 31–50.
Dunkl, I., Frisch, W., Kuhlemann, J., Brügel, A., 2009. Pebble population dating as an additional tool for provenance studies – examples from the Eastern Alps. Geol. Soc. Lond., Spec. Publ. 324, 125–140.
Elias, J., 1998. The Thermal History of the Ötztal-Stubai Complex (Tyrol, Austria/Italy) in the Light of the Lateral Extrusion Model. Institut und Museum für Geologie und Paläontologie der Univ, Tübingen.
Faupl, P., Wagreich, M., 1992. Cretaceous flysch and pelagic sequences of the Eastern Alps: correlations, heavy minerals, and palaeogeographic implications. Cretac. Res. 13, 387–403.
Flisch, M., 1986. Die Hebungsgeschichte der oberostalpinen Silvretta-Decke seit der mittleren Kreide. Bull. Ver. Schweiz. Pet.-Geol. Ing. 53, 23–49.
Franke, W., 2000. The mid-European segment of the Variscides: tectonostratigraphic units, terrane boundaries and plate tectonic evolution. Geol. Soc. Lond., Spec. Publ. 179, 35–61.
Franke, W., Żelaźniewicz, A., 2002. Structure and evolution of the Bohemian Arc. Geol. Soc. Lond., Spec. Publ. 201, 279–293.
Frisch, W., 1979. Tectonic progradation and plate tectonic evolution of the Alps. Tectonophysics 60, 121–139.
Froitzheim, N., Manatschal, G., 1996. Kinematics of Jurassic rifting, mantle exhumation, and passive-margin formation in the Austroalpine and Penninic nappes (eastern Switzerland). Geol. Soc. Am. Bull. 108, 1120–1133.
Fügenschuh, B., Seward, D., Mancktelow, N., 1997. Exhumation in a convergent orogen: the western Tauern window. Terra Nova 9, 213–217.
Fügenschuh, B., Schmid, S., 2005. Age and significance of core complex formation in a very curved orogen: Evidence from fission track studies in the South Carpathians (Romania). Tectonophysics 404, 33–53.
Gallhofer, D., Quadt, A., Peytcheva, I., Schmid, S.M., Heinrich, C.A., 2015. Tectonic, magmatic, and metallogenic evolution of the late cretaceous arc in the Carpathian-Balkan orogen. Tectonics 34, 1813–1836.
Gedeon-Rajetzky, M., 1973. Evaluation of the micromineralogical spectra of ancient fluvial sediments based on the analysis of recent detritus (in Hungarian). Bull. Hung. Geol. Soc. (Földtani Közlöny) 103, 285–293.
Glasmacher, U.A., Mann, U., Wagner, G.A., 2002. Thermotectonic evolution of the Barrandian, Czech Republic, as revealed by apatite fission-track analysis. Tectonophysics 359, 381–402.
Gleadow, A., 1981. Fission-track dating methods: what are the real alternatives? Nuclear Tracks 5, 3–14.
Gröger, H.R., Tischler, M., Fügenschuh, B., Schmid, S.M., 2013. Thermal history of the Maramureş area (Northern Romania) constrained by zircon fission track analysis: Cretaceous metamorphism and Late Cretaceous to Paleocene exhumation. Geol. Carpath. 64, 383–398.
Grundmann, G., Morteani, G., 1985. The young uplift and thermal history of the central Eastern Alps (Austria/Italy), evidence from apatite fission track ages. Jahrb. Geol. Bundesanst. 128, 197–216.
Hejl, E., 1997. 'Cold spots' during the Cenozoic evolution of the Eastern Alps: thermochronological interpretation of apatite fission-track data. Tectonophysics 272, 159–173.
Hejl, E., Grundmann, G., 1989. Apatit-Spaltspurendaten zur thermischen Geschichte der Nördlichen Kalkalpen, der Flysch- und Molassezone. Jahrb. Geol. Bundesanst. 132, 191–212.
Hejl, E., Coyle, D., Lal, N., Van den Haute, P., Wagner, G., 1997. Fission-track dating of the western border of the Bohemian massif: thermochronology and tectonic implications. Geol. Rundsch. 86, 210–219.
Hejl, E., Sekyra, G., Friedl, G., 2003. Fission-track dating of the south-eastern Bohemian massif (Waldviertel, Austria): thermochronology and long-term erosion. Int. J. Earth Sci. 92, 677–690.
Horváth, F., Musitz, B., Balázs, A., Végh, A., Uhrin, A., Nádor, A., Koroknai, B., Pap, N., Tóth, T., Wórum, G., 2015. Evolution of the Pannonian basin and its geothermal resources. Geothermics 53, 328–352.
Hubert, J.F., 1962. A zircon-tourmaline-rutile maturity index and the interdependence of the composition of heavy mineral assemblages with the gross composition and texture of sandstones. J. Sediment. Res. 32, 440–450.
Hurai, V., Marko, F., Tokarski, A.K., Świerczewska, A., Kotulová, J., Biroň, A., 2006. Fluid inclusion evidence for deep burial of the Tertiary accretionary wedge of the Carpathians. Terra Nova 18, 440–446.
Hurford, A.J., 1986. Cooling and uplift patterns in the Lepontine Alps South Central Switzerland and an age of vertical movement on the Insubric fault line. Contrib. Mineral. Petrol. 92, 413–427.
Janoušek, V., Wiegand, B.A., Žák, J., 2010. Dating the onset of Variscan crustal exhumation in the core of the Bohemian Massif: new U–Pb single zircon ages from the high-K calc-alkaline granodiorites of the Blatná suite, Central Bohemian Plutonic complex. J. Geol. Soc. 167, 347–360.
Juhász, G., Thamó-Bozsó, E., 2006. The mineral composition of the Pannonian sl Formations in the Great Hungarian Plain (II). Tendencies of the changes of the mineral composition of the Pannonian s.l. sands and sandstones and their geological significance. Bull. Hung. Geol. Soc. (Földtani Közlöny) 136, 431–450.
Kassambara, A., 2017. Practical Guide to Principal Component Methods in R: PCA, M (CA), FAMD, MFA, HCPC, Factoextra (Statistical tools for high-throughout data analysis).
Kempf, O., Matter, A., Burbank, D., Mange, M., 1999. Depositional and structural evolution of a foreland basin margin in a magnetostratigraphic framework: the eastern Swiss Molasse Basin. Int. J. Earth Sci. 88, 253–275.
Klein, T., Kiehm, S., Siebel, W., Shang, C., Rohrmüller, J., Dörr, W., Zulauf, G., 2008. Age and emplacement of late-Variscan granites of the western Bohemian Massif with main focus on the Hauzenberg granitoids (European Variscides, Germany). Lithos 102, 478–507.
Kounov, A., Schmid, S.M., 2013. Fission-track constraints on the thermal and tectonic evolution of the Apuseni Mountains (Romania). Int. J. Earth Sci. 102, 207–233.
Kováč, M., Král, J., Márton, E., Plašienka, D., Uher, P., 1994. Alpine uplift history of the Central Western Carpathians: geochronological, paleomagnetic, sedimentary and structural data. Geol. Carpath. 45, 83–96.
Král, J., 1977. Fission track ages of apatites from some granitoid rocks in West Carpathians. Geol. Zb. Geol. Carpath. 28, 269–276.
Králiková, S., Vojtko, R., Andriessen, P., Kováč, M., Fügenschuh, B., Hók, J., Minár, J., 2014a. Late Cretaceous–Cenozoic thermal evolution of the northern part of the Central Western Carpathians (Slovakia): revealed by zircon and apatite fission track thermochronology. Tectonophysics 615, 142–153.
Králiková, S., Vojtko, R., Sliva, U., Minár, J., Fügenschuh, B., Kováč, M., Hók, J., 2014b. Cretaceous—Quaternary tectonic evolution of the Tatra Mts (Western Carpathians): constraints from structural, sedimentary, geomorphological, and fission track data. Geol. Carpath. 65, 307–326.
Králiková, S., Vojtko, R., Hók, J., Fügenschuh, B., Kováč, M., 2016. Low-temperature constraints on the Alpine thermal evolution of the Western Carpathian basement rock complexes. J. Struct. Geol. 91, 144–160.
Krézsek, C., Bally, A.W., 2006. The Transylvanian Basin (Romania) and its relation to the Carpathian fold and thrust belt: Insights in gravitational salt tectonics. Mar. Pet. Geol. 23, 405–442.

Krobicki, M., Golonka, J., Aubrecht, R., 2003. Pieniny Klippen Belt: general geology and geodynamic evolution. In: Geology, Geophysics, Geothermics and Deep Structure of the West Carpathians and Their Basement. Polish Academy of Sciences.
Kuhlemann, J., Kempf, O., 2002. Post-Eocene evolution of the North Alpine Foreland Basin and its response to Alpine tectonics. Sediment. Geol. 152, 45–78.
Kuhlemann, J., Frisch, W., Dunkl, I., Székely, B., Spiegel, C., 2001. Miocene shifts of the drainage divide in the Alps and their foreland basin. Z. Geomorphol. 45, 239–265.
Kuhlemann, J., Frisch, W., Székely, B., Dunkl, I., Kázmér, M., 2002. Post-collisional sediment budget history of the Alps: tectonic versus climatic control. Int. J. Earth Sci. 91, 818–837.
Lexa, J., Seghedi, I., Németh, K., Szakács, A., Konečny, V., Pécskay, Z., Fülöp, A., Kovacs, M., 2010. Neogene-Quaternary volcanic forms in the Carpathian-Pannonian Region: a review. Open Geosci. 2, 207–270.
Lukács, R., Harangi, S., Guillong, M., Bachmann, O., Fodor, L., Buret, Y., Dunkl, I., Sliwinski, J., von Quadt, A., Peytcheva, I., Zimmerer, M., 2018. Early to Mid-Miocene syn-extensional massive silicic volcanism in the Pannonian Basin (East-Central Europe): eruption chronology, correlation potential and geodynamic implications. Earth Sci. Rev. 179, 1–19.
Lünsdorf, N.K., Kalies, J., Ahlers, P., Dunkl, I., von Eynatten, H., 2019. Semi-automated heavy-mineral analysis by Raman spectroscopy. Minerals 9, 385.
Magyar, I., Radivojević, D., Sztanó, O., Synak, R., Ujszászi, K., Pócsik, M., 2013. Progradation of the paleo-Danube shelf margin across the Pannonian Basin during the Late Miocene and Early Pliocene. Glob. Planet. Chang. 103, 168–173.
Malusà, M.G., Balestrieri, M.L., 2012. Burial and exhumation across the Alps–Apennines junction zone constrained by fission-track analysis on modern river sands. Terra Nova 24, 221–226.
Malusà, M.G., Resentini, A., Garzanti, E., 2016. Hydraulic sorting and mineral fertility bias in detrital geochronology. Gondwana Res. 31, 1–19.
Matenco, L., Andriessen, P., 2013. Quantifying the mass transfer from mountain ranges to deposition in sedimentary basins: source to sink studies in the Danube Basin–Black Sea system. Glob. Planet. Chang. 103, 1–18.
Matenco, L., 2017. Tectonics and exhumation of Romanian Carpathians: Inferences from kinematic and thermochronological studies, Landform dynamics and evolution in Romania. Springer, pp. 15–56.
Merten, S., Matenco, L., Foeken, J., Stuart, F., Andriessen, P., 2010. From nappe stacking to out-of-sequence postcollisional deformations: Cretaceous to Quaternary exhumation history of the SE Carpathians assessed by low-temperature thermochronology. Tectonics 29.
Merten, S., Matenco, L., Foeken, J., Andriessen, P., 2011. Toward understanding the post-collisional evolution of an orogen influenced by convergence at adjacent plate margins: Late Cretaceous–Tertiary thermotectonic history of the Apuseni Mountains. Tectonics 30.
Miller, C., Thöni, M., Konzett, J., Kurz, W., Schuster, R., 2005. Eclogites from the Koralpe and Saualpe type-localities, eastern Alps, Austria. Mitt. Österr. Mineral. Ges. 150, 227–263.
Molnár, B., 1964. Heavy mineral analysis of the sandy sediments of Hungarian rivers (in Hungarian). Bull. Hung. Hydrol. Soc. (Hidrológiai Közlöny) 44, 347–355.
Molnár, K., Lukács, R., Dunkl, I., Schmitt, A.K., Kiss, B., Seghedi, I., Szepesi, J., Harangi, S., 2019. Episodes of dormancy and eruption of the Late Pleistocene Ciomadul volcanic complex (Eastern Carpathians, Romania) constrained by zircon geochronology. J. Volcanol. Geotherm. Res. 373, 133–147.
Morton, A.C., Hallsworth, C., 1994. Identifying provenance-specific features of detrital heavy mineral assemblages in sandstones. Sediment. Geol. 90, 241–256.
Morton, A.C., Hallsworth, C.R., 1999. Processes controlling the composition of heavy mineral assemblages in sandstones. Sediment. Geol. 124, 3–29.
Moser, F., Hann, H., Dunkl, I., Frisch, W., 2005. Exhumation and relief history of the Southern Carpathians (Romania) as evaluated from apatite fission track chronology in crystalline basement and intramontane sedimentary rocks. Int. J. Earth Sci. 94, 218–230.
Nakapelyukh, M., Bubniak, I., Bubniak, A., Jonckheere, R., Ratschbacher, L., 2018. Cenozoic structural evolution, thermal history, and erosion of the Ukrainian Carpathians fold-thrust belt. Tectonophysics 722, 197–209.
Neubauer, F., Dallmeyer, R.D., Dunkl, I., Schirnik, D., 1995. Late cretaceous exhumation of the metamorphic Gleinalm dome, Eastern Alps: kinematics, cooling history and sedimentary response in a sinistral wrench corridor. Tectonophysics 242, 79–98.
Nemčok, M., Hok, J., Kovac, P., Marko, F., Coward, M., Madaras, J., Bezak, V., 1998. Tertiary extension development and extension/compression interplay in the West Carpathian mountain belt. Tectonophysics 290, 137–167.
Nicolae, I., 1992. Ages K-Ar de quelques ophiolites des Monts Apuseni du Sud et leur signification géologique (Roumanie). Geol. Alpine 68, 77–83.
Obbágy, G., Dunkl, I., Józsa, S., Silye, L., Arató, R., Lünsdorf, N.K., von Eynatten, H., 2021. Paleogeographic implications of a multi-parameter Paleogene provenance dataset (Transylvanian Basin, Romania). J. Sediment. Res. under review.
Oszczypko, N., 2006. Late Jurassic-Miocene evolution of the Outer Carpathian fold-and-thrust belt and its foredeep basin (Western Carpathians, Poland). Geol. Q. 50, 169–194.
Pană, D., Heaman, L., Creaser, R., Erdmer, P., 2002. Pre-alpine crust in the Apuseni Mountains, Romania: insights from Sm-Nd and U-Pb data. J. Geol. 110, 341–354.
Pécskay, Z., Lexa, J., Kovacs, M., 1995. Space and time distribution of Neogene-Quaternary volcanism in the Carpatho-Pannonian region. Acta Vulcanol. 7, 15–28.
Petrasová, K., Faryad, S.W., Jerabek, P., Zackova, E., 2007. Origin and metamorphic evolution of magnesite-talc and adjacent rocks near Gemerská Poloma, Slovak Republic. J. Geosci. 52, 125–132.
Plašienka, D., Grecula, P., Putiš, M., Kováč, M., Hovorka, D., 1997. Evolution and structure of the Western Carpathians: an overview. In: Geological Evolution of the Western Carpathians, pp. 1–24.
Plašienka, D., Broska, I., Kissova, D., Dunkl, I., 2007. Zircon fission-track dating of granites from the Vepor-Gemer Belt (Western Carpathians): constraints for the early Alpine exhumation history. J. Geosci. 52, 113–123.
Reiser, M., 2015. The Tectonometamorphic Evolution of the Apuseni Mountains during the Cretaceous. PhD. University of Innsbruck.
Reiser, M.K., Schuster, R., Spikings, R., Tropper, P., Fügenschuh, B., 2017. From nappe stacking to exhumation: cretaceous tectonics in the Apuseni Mountains (Romania). Int. J. Earth Sci. 106, 659–685.
Reiser, M.K., Săbău, G., Negulescu, E., Schuster, R., Tropper, P., Fügenschuh, B., 2019. Post-Variscan metamorphism in the Apuseni and Rodna Mountains (Romania): evidence from Sm–Nd garnet and U–Th–Pb monazite dating. Swiss J. Geosci. 112, 101–120.
Sachsenhofer, R.F., Dunkl, I., Hasenhüttl, C., Jelen, B., 1998. Miocene thermal history of the southwestern margin of the Styrian Basin: vitrinite reflectance and fission-track data from the Pohorje/Kozjak area (Slovenia). Tectonophysics 297, 17–29.
Sanders, C.A., Andriessen, P., Cloetingh, S., 1999. Life cycle of the East Carpathian orogen: Erosion history of a doubly vergent critical wedge assessed by fission track thermochronology. J. Geophys. Res. Solid Earth 104, 29095–29112.
Săndulescu, M., Krautner, H., Balintoni, I., Russo-Sandulescu, D., Micu, M., 1981. The structure of the East Carpathians, Guide Book to Excursion B1 of the Carpatho-Balkan Geological Association 12th Congress, Bucharest, pp. 1–92.
Schmid, S.M., Berza, T., Diaconescu, V., Froitzheim, N., Fügenschuh, B., 1998. Orogen-parallel extension in the Southern Carpathians. Tectonophysics 297, 209–228.
Schmid, S.M., Bernoulli, D., Fügenschuh, B., Matenco, L., Schefer, S., Schuster, R., Tischler, M., Ustaszewski, K., 2008. The Alpine-Carpathian-Dinaridic orogenic system: correlation and evolution of tectonic units. Swiss J. Geosci. 101, 139–183.
Schuller, V., 2004. Evolution and geodynamic significance of the Upper Cretaceous Gosau basin in the Apuseni Mountains (Romania) [Ph.D. thesis]: University of Tübingen, Tübingen, p. 112.
Schuller, V., Frisch, W., 2006. Heavy mineral provenance and paleocurrent data of the Upper Cretaceous Gosau succession of the Apuseni Mountains (Romania). Geol. Carpath. 57, 29.
Schuller, V., Frisch, W., Danišík, M., Dunkl, I., Melinte, M.C., 2009. Upper Cretaceous Gosau deposits of the Apuseni Mountains (Romania) – similarities and differences to the Eastern Alps. Austrian J. Sci. 133–145.
Seghedi, A., Berza, T., Iancu, V., Maruntiu, M., Gheorghe, O., 2005. Neoproterozoic terranes in the Moesian basement and in the Alpine Danubian nappes of the South Carpathians. Geol. Belg. 8 (4), 4–19.
Śmigielski, M., Sinclair, H., Stuart, F., Persano, C., Krzywiec, P., 2016. Exhumation history of the Tatry Mountains, Western Carpathians, constrained by low-temperature thermochronology. Tectonics 35, 187–207.
Sobczyk, A., Sobel, E.R., Georgieva, V., 2020. Meso–Cenozoic cooling and exhumation history of the Orlica-Śnieżnik Dome (Sudetes, NE Bohemian Massif, Central Europe): insights from apatite fission-track thermochronometry. Terra Nova 32, 122–133.
Stampfli, G., Marcoux, J., Baud, A., 1991. Tethyan margins in space and time. Palaeogeogr. Palaeoclimatol. Palaeoecol. 87, 373–409.
Staufenberg, H., 1987. Apatite fission-track evidence for postmetamorphic uplift and cooling history of the Eastern Tauern Window and the surrounding Austroalpine (Central Eastern Alps, Austria). Jahrb. Geol. Bundesanst. 130, 571–586.
Stöckhert, B., Brix, M.R., Kleinschrodt, R., Hurford, A.J., Wirth, R., 1999. Thermochronometry and microstructures of quartz—a comparison with experimental flow laws and predictions on the temperature of the brittle–plastic transition. J. Struct. Geol. 21, 351–369.
Stoica, A.M., Ducea, M.N., Roban, R.D., Jianu, D., 2016. Origin and evolution of the South Carpathians basement (Romania): a zircon and monazite geochronologic study of its Alpine sedimentary cover. Int. Geol. Rev. 58, 510–524.
Szabó, P., 1955. Origin of the late Pleistocene sandy strata on the Duna-Tisza Interfluve, based on their mineralogical composition (in Hungarian). Bull. Hung. Geol. Soc. (Földtani Közlöny) 85, 442–456.
Tari, G., Dövényi, P., Dunkl, I., Horváth, F., Lenkey, L., Stefanescu, M., Szafián, P., Tóth, T., 1999. Lithospheric structure of the Pannonian basin derived from seismic, gravity and geothermal data. Geol. Soc. Lond., Spec. Publ. 156, 215–250.
Thamó-Bozsó, E., Kovács, L.Ó., 2007. Evolution of Quaternary to modern fluvial network in the Mid-Hungarian plain, indicated by heavy mineral distributions and statistical analysis of heavy mineral data. Dev. Sedimentol. 58, 491–514.
Thamó-Bozsó, E., Juhász, G., Kovács Lajos, Ó., 2006. The mineral composition of the Pannonian sl Formations in the Great Hungarian Plain (I). The characteristics and origins of the Pannonian sl sands and sandstones. Bull. Hung. Geol. Soc. (Földtani Közlöny) 136, 407–429.
Torgerson, W.S., 1952. Multidimensional scaling: I. Theory and method. Psychometrika 17, 401–419.
Trautwein, B., Dunkl, I., Kuhlemann, J., Frisch, W., 2001. Cretaceous–Tertiary Rhenodanubian flysch wedge (Eastern Alps): clues to sediment supply and basin configuration from zircon fission-track data. Terra Nova 13, 382–393.
Uher, P., Broska, I., 1996. Post-orogenic Permian granitic rocks in the Western Carpathian-Pannonian area: geochemistry, mineralogy and evolution. Geol. Carpath. 47, 311–322.
Vamvaka, A., Siebel, W., Chen, F., Rohrmüller, J., 2014. Apatite fission-track dating and low-temperature history of the Bavarian Forest (southern Bohemian Massif). Int. J. Earth Sci. 103, 103–119.
Vermeesch, P., 2013. Multi-sample comparison of detrital age distributions. Chem. Geol. 341, 140–146.
Vermeesch, P., Resentini, A., Garzanti, E., 2016. An R package for statistical provenance analysis. Sediment. Geol. 336, 14–25.
Vermeesch, P., 2019. Exploratory Analysis of Provenance Data Using R and the Provenance Package. Minerals 9, 193.

Viola, G., Mancktelow, N.S., Seward, D., 2001. Late Oligocene-Neogene evolution of Europe-Adria collision: new structural and geochronological evidence from the Giudicarie fault system (Italian Eastern Alps). Tectonics 20, 999–1020.
Vojtko, R., Králiková, S., Jeřábek, P., Schuster, R., Danišík, M., Fügenschuh, B., Minár, J., Madarás, J., 2016. Geochronological evidence for the Alpine tectono-thermal evolution of the Veporic Unit (Western Carpathians, Slovakia). Tectonophysics 666, 48–65.
Winkler, W., Slaczka, A., 1992. Sediment dispersal and provenance in the Silesian, Dukla and Magura flysch nappes (Outer Carpathians, Poland). Geol. Rundsch. 81, 371–382.
Zattin, M., Andreucci, B., Jankowski, L., Mazzoli, S., Szaniawski, R., 2011. Neogene exhumation in the outer Western Carpathians. Terra Nova 23, 283–291.